Journal of Electronics and Electrical Engineering
https://ojs.wiserpub.com/index.php/JEEE

Review

A Comprehensive Review on Frequency Reconfigurable Antennas for 4G, 5G and sub-6 GHz Systems with Emerging Techniques

A. Y. Deshpande[1*], Madhavi Bhong[1*], Ajay Prudhvi Raj[2], Y. B. Thakare[1], K. P. Ray[2]

[1] Department of Electronics and Telecommunication Engineering, Pune Vidyarthi Griha's College of Engineering, Technology and Management, Pune, India
[2] Department of Electronics Engineering, Defense Institute of Advanced Technology, Pune, India
[*] Correspondence: aadesh.an4@gmail.com (A.Y.D.); madhavibhong@gmail.com (M.B.)

Received: 8 December 2025; **Revised:** 1 April 2026; **Accepted:** 9 April 2026; **Published:** 28 April 2026

Abstract: The rapid evolution of wireless communication systems across sub-6 GHz and millimeter Wave bands has intensified the demand for Frequency Reconfigurable Antennas (FRAs) capable of adaptive, multi-standard operation. This review presents a comprehensive performance-driven synthesis of reconfigurable patch antenna architectures developed from 1963 to 2026, with emphasis on recent advances after 2020. Reconfiguration techniques are systematically classified into electrical, mechanical, and metamaterial-based approaches and evaluated based on key performance parameters including tuning range, radiation efficiency, switching speed, biasing complexity, and structural footprint. Electrical methods employing PIN diodes, varactors, and RF-MEMS switches are analyzed alongside mechanical actuators, liquid-metal and phase-change materials, magneto-dielectric substrates, and metasurface-based mechanisms to establish critical trade-offs between actuation latency, power handling, and integration feasibility. A unified benchmarking framework incorporating comparative performance mapping and response-time frontiers is introduced to support informed design selection. Additionally, the emerging role of machine learning in reducing simulation overhead and enabling predictive optimization is discussed as a transformative paradigm in antenna engineering. The review concludes by outlining research challenges and hybrid strategies essential for 5G and future 6G adaptive communication systems.

***Keywords*:** Frequency Reconfigurable Antenna (FRA), Artificial Intelligence (AI), Machine Learning (ML), flexible antennas, Positive-Intrinsic-Negative (PIN) diodes, varactors, metamaterials

1. Introduction

Antennas play a fundamental role in modern wireless communication systems, serving as the critical interface between electronic circuits and free-space propagation. With the rapid evolution of compact, high data rate devices, antenna architectures must simultaneously satisfy constraints of miniaturization, cost-effectiveness, radiation efficiency, and multi-band operation. As wireless standards expand across sub-6 GHz and millimeter Wave (mmWave) spectra, the need for adaptive frequency behavior has become increasingly significant. Reconfigurable antennas address this demand by enabling dynamic modification of operating frequency, radiation characteristics, or polarization within a single compact structure. Table 1 summarizes the commonly used IEEE-defined frequency bands and their typical applications, highlighting the broad spectral landscape that modern antennas accommodate.

DOI: https://doi.org/10.37256/jeee.5120269368

The focus on antenna development in 4G, 5G, and sub-6 GHz wireless networks led to an exponential increase in demand for advanced antennas. The following paragraph describes the usage range of these wireless generations. The 4G band extends from 450 MHz to 2.6 GHz, penetrating into sub-6 GHz band due to the Long Term Evolution (LTE) of 4G. The 5G band operates in two main subdivisions, sub-6 GHz frequency (1 GHz to 6 GHz) and mmWave band of 24 GHz to 100 GHz. The sub-6 GHz band is a sweet spot for several domestic and industry standards, as it provides a balance between coverage, capacity, and speed [1].

Table 1. Commonly used IEEE RF and microwave frequency range and applications

Band name	Frequency range	Applications
VHF band	30 MHz–300 MHz	FM radio, duplex radios, TV, marine communication
UHF band	300 MHz–3 GHz	DTV, cellular networks, Bluetooth, RFID, GPS, Wi-Fi.
L-band	1 GHz–2 GHz	GPS/GNSS, GSM, 4G, radar, satellite TV.
S-band	2 GHz–4 GHz	Wi-Fi (2.4 GHz), 4G-LTE, radar, WiMax, satcomm.
C-band	4 GHz–8 GHz	Satcomm, military radar, Wi-Fi (5 GHz), WLAN.
X-band	8 GHz–12 GHz	Air traffic, defense radars, radio astronomy.
Ku-band	12 GHz–18 GHz	Satellite internet, DBS, radars.
K-band	18 GHz–27 GHz	5G, radars, satellite comm.
Ka-band	27 GHz–40 GHz	mmWave 5G, weather radars.

1.1 *Evolution of reconfigurable antennas*

• Before 1960: The commonly used antenna designs used in this period were the horn antennas, parabolic antennas, helical antennas and the log periodic antennas. Changing any parameter (for example, length of wire) for these types was a very slow, complex, and impractical process. However, in [2], a phased array format was proposed which was able to adjust its beam direction by reversing phase of the array with optical sensors.

• 1960–1980: In the early 1960's, diodes were used as switches for beam steering of arrays, as mentioned in [3]. With the onset of 1980's Microstrip antennas were introduced which made the direct integration of lumped components in the antenna design possible. This period also saw the first frequency and polarization agile antenna patented by Schaubert et al. presented in [4].

• 1980–2000: In this time frame varactor diodes were introduced in antenna design. They enabled easier control and continuous frequency tuning.

• 2000–2010: Micro-Electro-Mechanical Systems (MEMS) were introduced during this period. They increased dynamic switching speed, were cheaper in terms of cost,and easily available.

• 2010–Present (2026): This period saw advancement in usage of RF-MEMS, PIN diodes, varactors, etc. along with modifications in patch shapes that aimed to improve antenna radiation characteristics. This period also saw the emergence of metamaterials integrated as substrates, patches, and other antenna components. A recent trend in antenna design is to use ML Algorithms to optimize antenna parameters.

1.2 *Reconfigurable antennas*

As summarized in Figure 1, a reconfigurable antenna can modify its radiation parameters such as frequency, radiation pattern, and/or polarization dynamically and reversibly to accommodate varying system requirements. Reconfigurable antennas can support more than one wireless protocol, giving the same performance as multiple antennas. This reduces system cost, system complexity, makes the system compact, improves performance and efficiency of the system. Such an arrangement also allows the system to be software programmable, allowing the system to be narrow-band or wide-band, act as a single element or array as per the requirement of the application. Multifunctional antennas have the ability to

reconfigure multiple characteristics at the same time. Patch antennas are considered suitable for use as reconfigurable antennas due to their flexibility in operation, compact size, low cost of fabrication, and broadband characteristics.

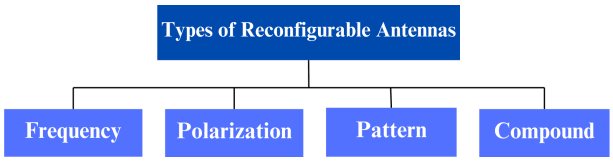

Figure 1. Types of reconfigurable antennas

The various methods to design a reconfigurable antenna is by connecting external devices, classified as electrical, mechanical, metamaterial, optical based reconfiguration techniques as shown in Figure 2. Electrical methods are the most widely used section due to their cost, accessibility, and flexibility of operation. A common practice to modify patch antenna parameters without using external devices or circuits is introducing slots (cuts), stubs (truncated patches), which also helps to achieve operation in multiple bands. A rectangular slot (sometimes U, F, H, L, I shaped) parallel to non-radiating edges tends to decrease the resonating frequency. The efficiency and gain of an antenna are inversely proportional to the length of the slot, whereas the bandwidth increases with the width of the slot. For multi-band reconfiguration, parasitic patches (with no direct feeding) or antenna arrays (multiplexed technique) are mounted on the substrate.

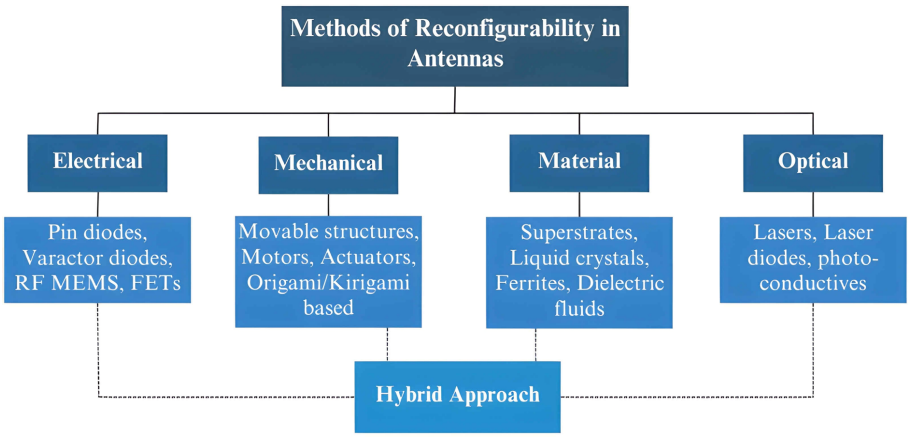

Figure 2. Methods of reconfigurability in antennas

The patch shapes with sharp edges are known to exhibit relatively narrow bandwidths, so as the edges are smoothened the bandwidth increases (with the circular shape exhibiting maximum bandwidth). The resonant frequency of the antenna is inversely proportional to the patch dimensions. The patch is usually composed of copper, but we can also use partially conducting materials such as salty water, dielectric fluids, and many other types of materials for improvised characteristics [5].

A low dielectric constant substrate encourages a wide bandwidth and boasts good radiation characteristics.It has been observed that increasing the thickness of the patch enhances gain, but reduces its directivity.

There are many feeding techniques to patch like direct feeding (microstrip feedline, Coaxial), indirect or contactless feeding (proximity coupling and aperture coupling). The impedance matching of the feed (typically 50 Ω) and antenna is required to transfer maximum power with minimum loss. In the Coplanar Waveguide (CPW) feed type, the ground is at the patch level near the feed network.

Tuning/Truncating the dimensions of the ground plane can improve the gain of a patch antenna (known as Defected Ground Structure (DGS)). The size of the ground plane contributes significantly to the tuning of the resonating frequency,

power efficiency, and directivity which is explained in [6]. Table 2 summarizes the general effect of the components of a patch antenna on its performance. It is important to note that these generalized effects can be varied depending on the requirement.

Table 2. Overall impact of component parameters on patch antenna performance

Antenna components	Component parameters	Physical variation	Effect on performance	Study reference
Substrate	Thickness (h)	Increases	Shifts resonant frequency towards the lower side as it increases, improving gain & BW.	[7–12]
		Decreases	Shifts frequency to upper end as decreases, with narrower BW for a fixed er, improving impedance matching.	
	Relative permittivity (ε_r)	Increases	Gain enhancement with increased directivity and compactness.	[9, 13]
		Decreases	More impedance is offered for higher resonance modes and overall efficiency is improved.	
	Loss tangent (δ)	Increase, decrease	Should be as low as possible for minimum dielectric losses.	
Ground	Location	Beneath patch	Better impedance matching and good efficiency with a stable radiation pattern.	[14–16]
		CPW	Enhances BW and gain in trade-off with spurious coupling.	
	Modification	No ground	Preferred for compact size, may reduce performance.	
		Truncations, reduced width, slots	Alters surface current, resulting in polarized propagation and improving performance, achieving reconfigurability.	
Feed	Type	Mircostrip, coaxial, coupling	Depends on the need of design specifications.	[17, 18]
	Width	Microstrip	Change in width affects impedance matching.	
Patch	Size	Increases, decreases	For lower resonances (UHF), size is large compared to higher resonances.	[17, 19]
	Shape	For standard shapes	For edged shapes, relatively narrower BW is obtained compared to edge-less shapes (like circular).	[20]
		For fractal shapes	Compact, wider BW and more gain.	
	Modification	Slots	Cuts in patch alters surface current, improving gain, directivity, impedance matching and multi-band resonance.	[21]
		Stubs	Acts as tuning elements of BW, pattern and polarization. Suppresses unwanted harmonics.	[22]
		Parasitic patches	Performance improvement of design, redirectors.	[23, 24]

1.3 *Emerging techniques of FRAs*

The historical evolution of antenna architectures demonstrates a progression toward various elements utilized for the parametric reconfigurability of standard patch designs as mentioned in section 1.1. Over the last decade, the escalation in design complexity and the demand for higher computational power have become increasingly prominent. Standard validation of these designs often relies on established electromagnetic (EM) solvers, such as CST Studio Suite, Ansys HFSS, Altair FEKO, and Keysight ADS/EMPro. These platforms provide robust analysis by solving Maxwell's equations in various numerical forms. However, these full-wave simulation techniques are inherently computationally demanding and

time-consuming, constituting a major bottleneck in the rapid prototyping cycle, as illustrated in the traditional workflow segment of Figure 3.

Rapid advancement in AI has established ML and Deep Learning (DL) as powerful leverages for the design and optimization of antenna parameters. Once a model is precisely trained for a specific antenna geometry, the time required for performance calculation and resource utilization is significantly reduced, improving overall design efficiency [25]. A systematic overview of such techniques is presented in [26].

The ML-based framework for antenna design, as summarized in Figure 3, begins with the requirement of a high-fidelity dataset. Typically, a dataset comprising 50 to 200 similar antenna designs and their performance metrics is necessary for shape optimization; however, the generation of training data remains a critical constraint as it still necessitates the initial use of traditional EM solvers [27]. Data is generally partitioned, with 70%-80% utilized for model training and the remainder reserved for validation.

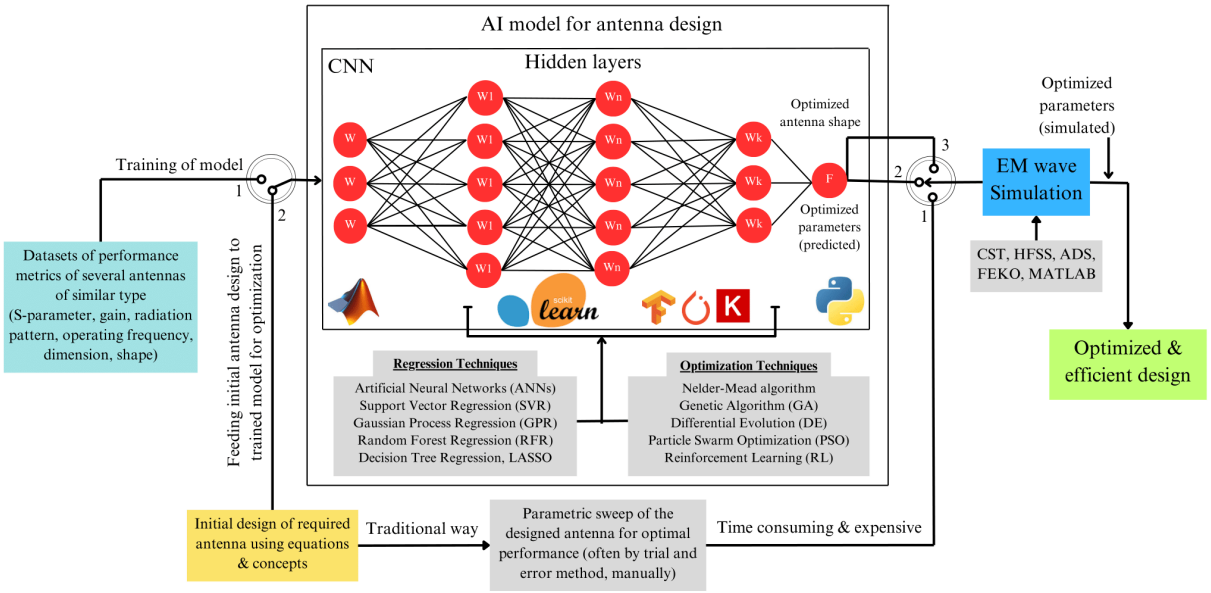

Figure 3. A comparative workflow of traditional antenna design versus ML-assisted optimization strategies

Algorithm selection is strategically determined by the design objective and dataset characteristics. For instance, Gaussian Process Regression (GPR) is preferred for modeling computationally expensive antennas when simulation data is sparse, as it provides unique uncertainty quantification to guide smart sampling. Conversely, Artificial Neural Networks (ANN) are optimal for modeling complex non-linearities in multi-band responses where large-scale datasets are available. Ensemble methods like Random Forest Regression (RFR) provide critical design insight through feature importance analysis, identifying which physical parameters (e.g., slot dimensions or stub lengths) most significantly impact the resonant frequency. Within these architectures, activation functions such as Rectified Linear Unit (ReLU), Sigmoid, and Tanh introduce the necessary non-linearity, allowing the model to adjust internal weights based on input scalability and prediction errors.

The objective of this review is to provide a performance-driven synthesis of Frequency Reconfigurable patch Antenna (FRA) architectures by systematically correlating actuation mechanisms with practical performance metrics such as tuning range, radiation efficiency, switching speed, biasing complexity, and structural footprint. Unlike conventional surveys that primarily categorize techniques, this work establishes a comparative evaluation framework through performance mapping, radar-based benchmarking, and frontier analysis of response time versus operational voltage.

Furthermore, this review integrates recent advancements in metamaterial engineering and machine learning-assisted optimization, highlighting the transition from hardware-centric tuning toward intelligent, predictive design methodologies.

By consolidating developments from 1963 to 2026, with emphasis on post-2020 innovations, this paper identifies emerging hybrid architectures and outlines research frontiers critical for 5G, mmWave, satellite-on-the-move, and future 6G wireless systems.

The context of this paper is organized into six sections. Section 1 is the introduction that discusses the basic history of reconfigurable antennas with emerging techniques. Section 2 focuses on Electrical methods of reconfigurability. Section 3 highlights recently advanced mechanical approaches for frequency tuning. Section 4 briefs on metamaterial based reconfigurability. Section 5 presents improvements in design and their procedures, along with advantages and challenges. It also highlights potential frontiers in antenna development. Finally, Section 6 concludes with the topic and the literature reviewed in this paper.

2. Electrical reconfigurable antennas

Modern wireless communication systems demand high data throughput while maintaining low power consumption and compact form factors as summarized in Table 2, FRAs have emerged as a practical solution to meet these requirements, predominantly through the incorporation of lumped tuning elements. Electrical reconfiguration is commonly achieved by integrating RF-MEMS, varactor diodes, and Positive-Intrinsic-Negative (PIN) diodes into the radiating structure. These components enable dynamic frequency control by modifying the effective electrical length and current distribution of the antenna surface. The comparative advantages of these lumped switching elements are illustrated in Figure 4.

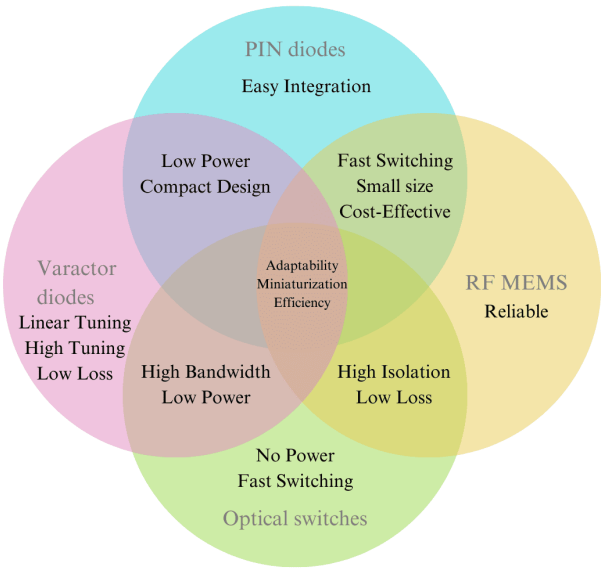

Figure 4. Advantages of lumped switches

2.1 *PIN diodes*

PIN diodes remain one of the most widely adopted switching elements in electrically reconfigurable antennas due to their low cost, compact size, fast switching speed, and ease of biasing integration. Their operation relies on transitioning between low resistance (ON) and high impedance (OFF) states, which alters the effective current path and electrical length of the radiating structure. This enables discrete frequency tuning, pattern modification, and multiband operation while maintaining structural simplicity. However, their inclusion may introduce ohmic losses and bias network complexity, particularly in designs employing multiple switching elements.

Flexible and textile-based implementations demonstrate the adaptability of PIN diode-based architectures in conformal and wearable systems. The conformal tri-band antenna in [28] exhibits broadband behavior enabled by semi-circular and rectangular stubs that enhance higher-order resonances and impedance bandwidth. Notably, mechanical bending improves gain and radiation efficiency due to favorable surface current redistribution, while maintaining stable resonant characteristics, highlighting the robustness of PIN diode-based tuning in flexible environments. Similarly, the truncated rectangular patch design in [29] achieves multiple reconfigurable states with circular polarization, where the use of a slotted ground and felt substrate enhances impedance matching and flexibility with minimal performance degradation.

A comparative study in [30] demonstrates that textile-based implementations provide mechanical adaptability with moderate gain, although frequency stability is slightly affected due to variations in substrate permittivity under deformation. Wearable designs such as [31] further extend this concept by enabling simultaneous frequency and polarization reconfiguration, making them suitable for body-centric wireless communication systems.

PIN diode integration is also effective in mmWave applications where compact switching is required. The design in [32] demonstrates wide tunability in the mmWave band using structural modifications such as diagonal truncation and stub loading to control current distribution and impedance bandwidth. However, this introduces trade-offs in radiation pattern stability. Similarly, beamwidth-reconfigurable designs such as [33] employ PIN-controlled parasitic elements to achieve simultaneous frequency and radiation pattern reconfiguration, highlighting the capability of PIN diodes in high-frequency adaptive systems.

Pattern and radiation control capabilities are further enhanced by the integration of parasitic elements. The Yagi-Uda antenna in [34] demonstrates wide-angle beam steering while maintaining high radiation efficiency, where PIN diodes effectively modify the electrical length of parasitic directors to enable dynamic pattern control without mechanical movement. Similarly, slot-loaded configurations such as [35] achieve notch-band tuning through PIN-controlled current path modification, highlighting the capability of PIN diodes in simultaneous frequency and pattern reconfiguration within compact structures.

PIN diode-based reconfigurable antennas are also highly effective in Internet of Things (IoT) and low-power communication systems. The spiral resonator antenna in [36], shown in Figure 5, enables compact multi-band operation with high radiation efficiency, where the spiral geometry supports miniaturization without significant performance degradation. Similarly, multiband UWB designs such as [37], shown in Figure 6, demonstrate strong isolation between radiating elements, making them suitable for compact multi-radio platforms. DNA-shaped patch geometries in [38] further enhance performance by improving current distribution through ground slot modifications, enabling efficient multiband operation in complex antenna structures.

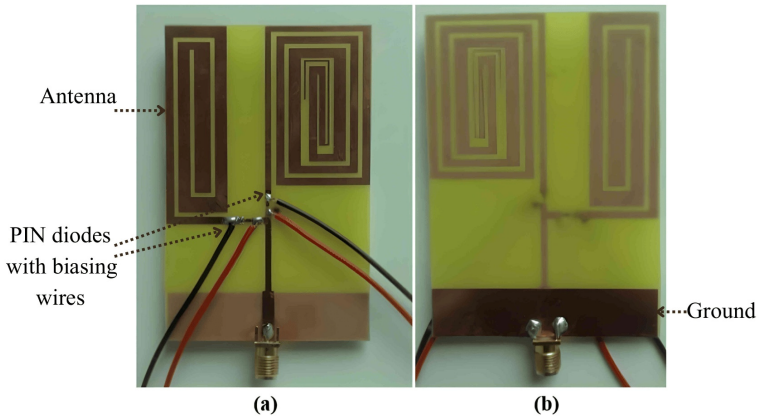

Figure 5. Prototype of the PIN diode reconfigurable rectangular spiral resonator antenna presented in [36]. (a) Front view, (b) back view. Adapted under CC BY 4.0

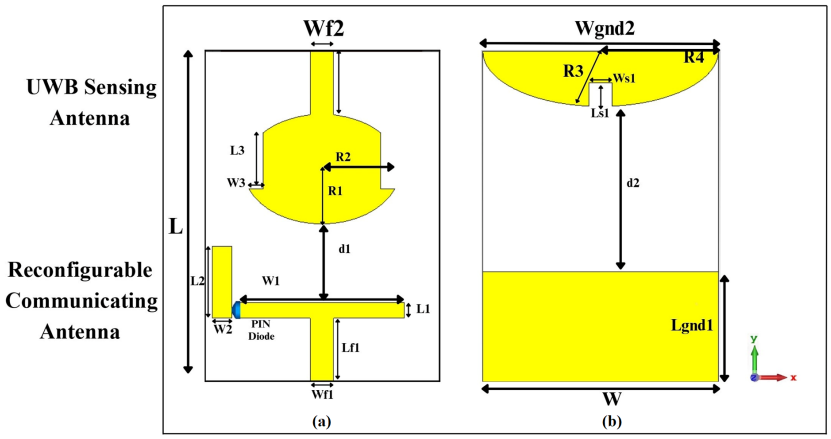

Figure 6. Multi-band cognitive radio reconfigurable antenna presented in [37]. (a) Front view, (b) Back view. Original figure licensed under CC BY-SA 4.0. This adapted figure is licensed under CC BY-SA 4.0

The use of multiple PIN diodes enables greater tuning flexibility but introduces trade-offs in efficiency and circuit complexity. For instance, the concentric circular patch design in [39] demonstrates extreme multiband capability by achieving a large number of resonant states across multiple frequency bands. However, increasing the number of switching elements leads to higher insertion loss and requires careful bias network design to mitigate efficiency degradation.

Flexible biomedical-oriented designs further highlight the adaptability of PIN diode-based tuning. The stub-loaded antenna in [40], shown in Figure 7, incorporates a CPW-fed structure that ensures stable radiation and impedance while bending, while a PIN-controlled stub allows frequency reconfiguration without structural changes.

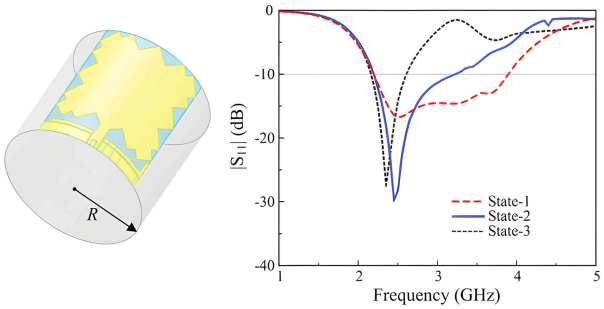

Figure 7. Stub-loaded flexible reconfigurable antenna demonstrating bending radius and its S11 response, reported in [40]. (CC BY-NC-ND 4.0)

Waveguide-integrated solutions such as [41] utilize multiple PIN diodes within an SIW cavity to achieve reconfigurable operation, offering high efficiency at higher frequencies. However, performance degrades at lower frequencies due to increased ohmic losses introduced by multiple switching elements and slot structures, highlighting a key limitation of PIN diode-based designs in highly complex architectures.

MIMO implementations such as [42], shown in Figure 8, further extend reconfigurability by enabling wide spectral coverage with high isolation and efficiency. The use of orthogonal patch configurations combined with PIN-controlled tuning enhances spectral flexibility, making such designs suitable for modern multi-band communication systems.

Material-assisted approaches are also explored to improve antenna performance. In [43], a graphene-based rectangular patch fabricated on a multilayer substrate supports multiple resonant modes, where the improved effective conductivity enhances radiation efficiency. Graphene offers advantages such as reduced weight, lower operating temperature, and environmental compatibility compared to conventional conductors; however, its relatively lower conductivity may limit achievable gain in high-power applications.

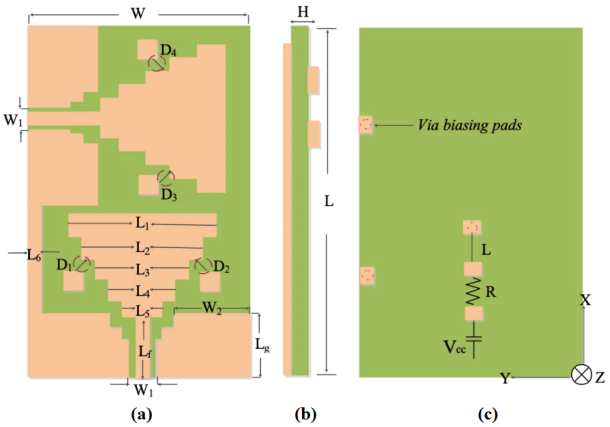

Figure 8. Geometry of the CPW-fed PIN diode reconfigurable antenna presented in [42]. (a) Front view, (b) side view, (c) back view. (CC BY NC-ND 4.0)

Overall, PIN diode-based reconfigurable antennas offer an effective balance between performance, cost, and implementation complexity. Their fast switching speed, compact size, and compatibility with planar fabrication make them suitable for sub-6 GHz, mmWave, wearable, IoT, and MIMO applications. A detailed analysis of the key performance parameters for PIN diode based frequency reconfiguration has been presented in Table 3.

Optical switching represents an emerging reconfiguration approach that eliminates the need for conventional electrical bias networks by exploiting photo-sensitive materials or light-dependent components. This approach reduces RF interference from bias lines and can enhance radiation efficiency. A representative Light Dependent Resistor (LDR)-based design [44], demonstrates frequency tuning through light-controlled resistance variation. A meandered split ring resonator patch composed of four unit cells is integrated with LDRs, as shown in Figure 9. Each unit cell connects to the feedline through an LDR, and incident light controls the effective resistance of the switching elements. The selective activation of unit cells modifies the effective electrical length of the antenna, enabling frequency reconfiguration. Since no direct biasing circuitry is required, the design minimizes parasitic effects and achieves a maximum gain of 8 dBi. The absence of metallic bias lines also improves radiation efficiency by reducing unwanted current leakage paths. Hence LDRs are particularly attractive in applications where electromagnetic interference must be minimized.

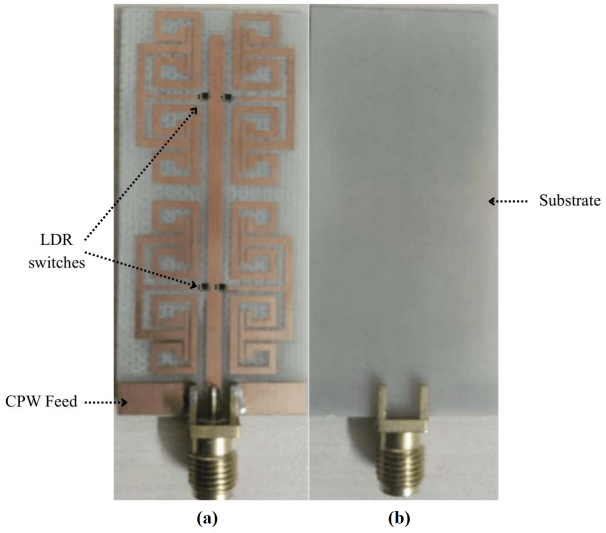

Figure 9. Prototype of reconfigurable meandering antenna with integrated LDR switches reported in [44]. a) Front view, b) back view. Adapted under CC BY 4.0

Table 3. Summary of the state of the art electrically reconfigurable antennas using PIN diodes of sub-Section 2.1

Ref	Frequency Range (GHz)	Substrate (ε_r) (height)	Total Dimension (mm^2)	Feed Type	Patch shape	Switches used	Peak Gain (dBi)	Applications
[29]	1.57, 1.67, 1.68, 2.43, 2.50, 2.55	Felt (ε_r = 1.22) (h = 1.7 mm)	113 x 99	Microstrip	Rectangular with diagonally cut slots	3 PIN diodes	4.8	GPS, Wi-Fi
[31]	2.45, 0.92	Jean (ε_r = 1.7) (h = 1 mm)	60 x 70	Microstrip	Circular with a C shaped parasitic patch	4 PIN diodes	1.09	Wearable technology
[45]	0.89, 1	FR4 (ε_r = 4.4) (h =1.59 mm)	74 x 52	Microstrip	Rectangle	1 silicon switch	N/A	Cellular networks, bluetooth
[46]	2.45–2.83	Rogers 4003 (ε_r = 3.55) (h = 3 mm)	240 x 120	Coaxial	Rectangular patch with a parasitic pixel layer	60 PIN diodes	6.4	Wi-Fi
[38]	4.68–6.12, 0.988 & 4.58, 2.67 & 3.36 & 4.76	Rogers 5870 (ε_r = 2.33) (h = 0.787 mm)	80 x 80	Microstrip	DNA-shape	2 PIN diodes	3.36	WLAN, 5G, WiMax, LTE
[39]	5.06∼17.58, 4.97∼17.3, 2.4∼19, 5.1∼17.48	FR4 (ε_r = 4.2) (h = 1.6 mm)	27 x 31.1	Microstrip	Concentric circles	2 PIN diodes	8 (dB)	ISM, Wi-Fi, LTE
[47]	4.4, 2.45, 3.5 & 4.8, 2.5 & 4.5	Rogers 5880 (ε_r = 2.2) (h = 0.254 mm)	30 x 25	CPW	Triangular patch with semicircular protrusion	2 PIN diodes	3.5	ISM, WLAN, WiMAX, and sub 6GHz 5G
[48]	1.229, 1.575 & 3.34	FR4 (ε_r = 4.3) (h = 1.6 mm)	54.6 x 54.6	Microstrip	Rectangle	1 PIN diode	7.035	GPS, Wimax
[49]	1.82–3.61 & 5.24–12.43	FR4 (ε_r = 4.4) (h = 1.6 mm)	66.4 x 66.4	Microstrip	Dodecagon with 3-delta structure	4 PIN diodes	4.14	ISM band, WiFi, WiMax,WLAN, PCS
[28]	2.47, 5.25, 8.1, 2.76–8.1	Rogers 5880 (ε_r = 2.1) (h = 0.254 mm)	25 x 35	CPW	Two semi-circles with a rectangle	1 PIN diode	5.8	ISM, UWB, WLAN
[41]	2.406–2.424, 5.683–6.005	Rogers 5880 (ε_r = 2.2) (h = 1.575 mm)	53.5 x 53.5	Coaxial	Rectangular patch, ring and slot, posts	12 PIN diodes	6.74	S & C bands
[30]	2.34, 3.56, 5.32 3.22, 4.99, 7.35 5.15, 7.26	FR4 (ε_r = 4.4) (h = 0.8 mm) Jean (ε_r = 1.7)	20 x 20	Microstrip	Square patch with E-slot	1 PIN diode	3.8	Bluetooth, WiMAX, WLAN
*[50]	1–7	FR-4 (ε_r = NA) (h = 1.5 mm)	84 x 64	Coaxial	Split-ring patch sim-card shape with metamaterial	3 PIN diodes	7.94	WiFi, WLAN, WiMAX, 5G
*[51]	3.3–4.2	FR-4 (ε_r = 4.4) (h = 1.6 mm)	40 x 42	Microstrip	Monopole, serpentine	1 PIN diode	2	Wireless sensor nodes, LoRa
[32]	27.81–34.56, 27–33.42, 29.62–34.55, 25.95–32.25	Rogers 6002 (ε_r = 2.94) (h = 0.76 mm)	7.7 x 5	Microstrip	Triangular patch with L and rectangular stubs	2 PIN diodes	6 (dB)	5G mmWave spectrum
[33]	27.2–32	Rogers 5880 (ε_r = 2.2) (h = 0.787 mm)	20 x 20	Microstrip	Circular patch, inclined rectangular slot, 3 arced parasitic patches	3 PIN diodes or 3 GeTe strips	9.1	beam steering, beam width, compact, 5G

Table 3. Cont.

Ref	Frequency Range (GHz)	Substrate (ε_r) (height)	Total Dimension (mm^2)	Feed Type	Patch shape	Switches used	Peak Gain (dBi)	Applications
[52]	2.08–5.53	FR4 (ε_r = 4.3) (h = 1.6 mm)	22 x 16	Microstrip	Rectangular spiral	2 PIN diodes or 2 SPDT switches	N/A	Sub-6G, Wi-Fi, bluetooth, WLAN
[53]	4.76–7.82, 4.5–4.8, 3.11–3.77, 2.24–2.66 & 5.87–6.9	FR4 (ε_r = 4.4) (h = 1.6 mm)	35 x 35	Microstrip	Planar monopole G-shape	3 PIN diodes	4.91	sub-6G, WLAN, Wi-Fi, C-band
[34]	4.71–5.84, 3.44–4.17, 2.61–3.13, 2.08–2.27	Rogers 5870 (ε_r = 2.33) (h = 0.787 mm)	38 x 40	Microstrip	Planar Yagi-Uda type	5 PIN diodes	3.72	5G New Radio bands, sub-6G
[40]	2.2–4.11 2.2–3.02 2.2–2.55	Rogers 5880 (ε_r = 2.2) (h = 0.127 mm)	8 x 32	CPW with bias-T network	Square with rectangular stubs	2 PIN diodes	2.58	Bio-medical imaging, Radar UWB
[42]	2.8, 3.5, 4.9–7.6, 8.6–13.4; 2.5–4.6, 6.1–8.5, 1–11.8; 2.5–4.3, 6.3–11.4, 12.4–14	FR4 (ε_r = 4.3) (h = 1.6 mm)	32 x 26	CPW (2 MIMO)	2 Tapered rectangular patch	4 PIN diodes	6.2	WiMAX, WLAN, X-band
[36]	0.433, 0.868, 0.915	FR4 (ε_r = 4.4) (h = 0.6 mm)	80 x 50	Microstrip	2 rectangular spirals	2 PIN diodes	2	LoRa, IOT, 4G
[54]	2.3–2.5, 5–6.2, 2–11	FR4 (ε_r = 4.4) (h = 2 mm)	45 x 40	Microstrip	elliptical patch with integrated feed network filter antenna	5 PIN diodes	3 (dB)	WLAN, WiMax
[55]	1.33–8.7	FR4 (ε_r = 4.4) (h = 1.6 mm)	47 x 37	Microstrip	Rectangular patch with modified ground	3 PIN diodes	10.13 (dB)	WLAN, WiFi, WiMax, L,S, C bands, UWB
[43]	5.17 & 6.13, 5.17 & 6.13 & 3.03	Polyamide (ε_r = 3.5) (h = 0.25 mm) PVC foam (ε_r = 1.5) (h = 1.35 mm)	54 x 46	Coaxial	Rectangular	1 PIN diode	2.09	Satellite broadcasting systems
[44]	1.8∼5.8, 2.5∼4.8, 1.3 ∼5.8, 2.5 ∼4.8	Taconic RF 3 (ε_r = 4.3) (h = 1.67 mm)	51 x 24	CPW	4 single split ring resonators	4 LDRs	11.6	Wireless communication
[56]	2 ∼16	FR4 (ε_r = 4.4) (h = 1.5 mm)	31 x 42	Microstrip	Slot and stub modified rectangle	2 PIN diodes	2.27 (dB)	S, C, X, Ku bands
[57]	3.3 & 5/5.8 & 6.6 & 9.9 & 15.9	FR4 (ε_r = 4.3) (h = 1.6 mm)	44 x 39	Vertex fed	Octagonal split ring resonator	1 PIN diode	4.1	WLAN, WiMax, C, X, Ku band
[37]	2.72–23.8, 7.925, 13.16, 14.48	FR4 (ε_r = 4.3) (h = 1.6 mm)	30 x 42	Microstrip (2 MIMO)	Elliptical and T-shape with rectangular vertical stub	1 PIN diode	8.5 (dB)	Cognitive radio, WiMax, radars

Note: N/A indicates Not Available; * represents ML assisted design.

2.2 *RF-MEMS*

RF-MEMS switches offer an alternative to semiconductor-based tuning elements by providing low insertion loss, high isolation, and excellent linearity at microwave and millimeter-wave frequencies. Unlike PIN diodes, RF-MEMS operate through electrostatic actuation, resulting in near-zero DC power consumption and reduced parasitic capacitance. These characteristics make them particularly suitable for high-frequency and high-efficiency reconfigurable antenna systems, although switching speed and fabrication complexity remain limiting factors.

In [58], RF-MEMS-based reconfigurability is demonstrated using a large-scale patch array with MEMS-controlled interconnections, enabling multiple discrete operating states. The array configuration highlights the capability of RF-MEMS in wideband and multi-band applications while maintaining low insertion loss. Figure 10 represents the simulated reflection coefficient for the proposed design. Minor discrepancies between simulated and measured results are attributed to fabrication tolerances and actuation variability, which remain practical challenges in MEMS-based systems.

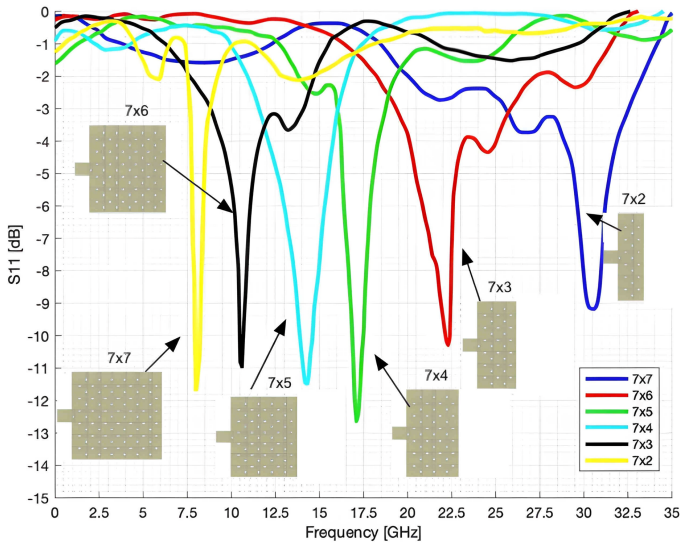

Figure 10. Simulated reflection coefficient results of the RF-MEMS reconfigurable rectangular antenna array by connected gold pads reported in [58] (CC BY 4.0)

Continuous tuning behavior is demonstrated in [59], where an RF-MEMS actuator enables fine frequency control through voltage variation. The use of an optimized CPW-to-microstrip transition minimizes parasitic discontinuities and improves impedance matching. Although the achievable tuning range is relatively narrow compared to PIN-based multi-state designs, the approach offers superior linearity and reduced loss, making it suitable for high-frequency precision applications.

Pixel-based reconfigurable structures further demonstrate the flexibility of MEMS integration. In [46], dynamically reconfigurable geometries are achieved by interconnecting parasitic pixel elements, effectively modifying the electrical length of the antenna. While this approach enhances tuning flexibility, it introduces trade-offs in bandwidth due to coupling limitations, requiring careful optimization of inter-layer spacing.

Single Pole Double Through (SPDT)-based MEMS implementations also reduce parasitic losses in multi-state configurations. The spiral geometry in [52] demonstrates compact reconfigurability with reduced switching loss while maintaining stable radiation characteristics. This highlights a key advantage of RF-MEMS in preserving radiation performance during reconfiguration.

Overall, RF-MEMS-based reconfigurable antennas, demonstrate superior performance in terms of insertion loss, isolation, and linearity, particularly at microwave and millimeter-wave frequencies. Their ability to maintain high radiation efficiency makes them attractive for precision communication systems, phased arrays, and high-frequency applications.

However, limitations such as slower switching speed, higher actuation voltage requirements, fabrication complexity, and long-term reliability concerns restrict their widespread deployment in low-cost or highly dynamic systems. Consequently, RF-MEMS are best suited for applications where low loss and high-frequency stability are prioritized over rapid switching and cost constraints.

2.3 *Varactor diodes*

Varactor diodes enable continuous frequency tuning through voltage-controlled capacitance variation. Unlike PIN diodes, which provide discrete ON-OFF states, varactors offer analog reconfigurability, making them particularly suitable for fine frequency adjustment and adaptive bandwidth control. However, their nonlinear characteristics and biasing sensitivity may introduce harmonic distortion and reduced power handling capability.

The design in [54] demonstrates dynamic bandwidth control by integrating a Band-Pass Filter (BPF) within the feed network. The use of an elliptical patch enables ultra-wideband behavior through improved surface current distribution and impedance matching, while harmonic suppression introduced by the BPF allows narrow-band operation. This highlights the effectiveness of combining feed-network engineering with varactor-based tuning to achieve adaptable bandwidth characteristics.

Similarly, [60] presents a compact inverted C-shaped radiator employing a varactor diode for continuous frequency tuning, enabling smooth spectral agility compared to discrete PIN diode switching. However, this approach introduces challenges such as biasing sensitivity and potential nonlinear effects. Feed-integrated varactor configurations further enhance impedance stability. In [61], a tunable BPF embedded within a T-shaped stub enables reconfigurable operation through voltage-controlled capacitance variation, demonstrating that placing varactors within the feed structure can improve tuning flexibility without directly modifying the radiating patch.

The use of multiple varactors, as shown in [62], increases tuning flexibility but introduces trade-offs in terms of insertion loss and radiation efficiency due to additional parasitic capacitance and biasing complexity.

Wearable implementations such as [63] extend varactor-based reconfiguration to flexible platforms using slotted ground structures and split-ring resonator (SRR) configurations. These designs enable multiband operation while exploring advanced material properties such as double-negative behavior, which is discussed further in later sections.

Overall, varactor-based reconfigurable antennas provide smooth and continuous frequency tuning with relatively simple integration into planar structures. They are particularly effective in adaptive communication systems and cognitive radio applications requiring fine frequency agility, as illustrated in Table 4. Nevertheless, nonlinear effects, limited power handling, and potential harmonic generation must be carefully managed to preserve signal integrity.

Table 4. Summary of the state of the art electrically reconfigurable antennas using RF-MEMS and varactor diodes and hybrid of sub-Section 2.2, 2.3

Ref	Frequency Range (GHz)	Substrate (ε_r) (height)	Total Dimension (mm^2)	Feed Type	Patch shape	Switches used	Peak Gain (dBi)	Applications
RF-MEMS-based Antennas								
[58]	7.6–31	Silicon wafer (ε_r ~11.9) (h = 0.65 mm)	5.23 x 5.23	Network	Array of 7x7 square patches	85 RF MEMS	N/A	FPGA, mmWave 5G, cubesat
[59]	15.75–16.05	Pyrex 7740 glass (ε_r = 4.6) (h = 0.5 mm)	4.3 x 4.3	CPW with bias-T network	Square patch with rectangular stub	5 RF MEMS	N/A	Ku-band
[64]	2–2.6, 2.6–3.2	Rogers 5880 (ε_r = 2.2) (h = 1.574 mm) Foam (ε_r = 1) (h = 10 mm)	100 x 120	Coaxial	E-shaped	2 RF-MEMS	10.46 (dB)	Cognitive Radio

Table 4. Cont.

Ref	Frequency Range (GHz)	Substrate (ε_r) (height)	Total Dimension (mm^2)	Feed Type	Patch shape	Switches used	Peak Gain (dBi)	Applications
Varactor-based Antennas								
[60]	5–6, 5.2–6.4, 5.4–6.6	Rogers 5880 (ε_r = 2.2) (h = 0.8 mm)	30 x 20	Microstrip	Inverted C on top of inverted L	1 Varactor	5.2	Sub 6GHz
[61]	1.68–1.73, 3.85–5.58, 4.26–5.94	Rogers 3003 (ε_r = 3) (h = 0.762 mm)	40 x 40	Microstrip	Square patch, rectangular strip, H&T-stub filter antenna	1 Varactor	3.1 (dB)	Cognitive Radio
[62]	3.29–4.01, 5.35–7	FR4 (ε_r = 4.4) (h = 1.6 mm)	33.9 x 38	Coaxial	Rectangular patch, 4 small rectangular parasitic patches	4 varactors	4.5	Cognitive radio, S & C band
*[65]	0.5–7.5	FR-4 (ε_r = 4.4) (h = 1.57 mm)	N/A	Coaxial	Four coupled patches	1 Varactor	N/A	Multi-band application
[35]	2.9∼18.3, 3.06∼18.1, 2.58∼17.85	FR4 (ε_r = 4.4) (h = 0.8 mm)	30 x 30	CPW	semi-circular and rectangular with inverted U-shape slot	2 PIN diodes, 1 varactor	4 (dB)	WiMAX, WLAN, C-band
[66]	3.04–5.89	N/A (ε_r = 2.65) (h = 1 mm)	50 x 45	Mircostrip	Bow-tie shape	2 PIN diodes, 2 varactors	4.44	UWB, cognitive radio

Note: N/A indicates Not Available; * represents ML assisted design.

2.4 *Machine Learning assisted design optimization*

Machine Learning (ML) techniques have recently emerged as powerful tools for antenna design optimization, enabling rapid prediction of resonant frequency, gain, bandwidth, and impedance characteristics without relying solely on computationally intensive full-wave simulations. By learning nonlinear relationships between geometric parameters and electromagnetic responses, ML models significantly reduce design time while maintaining high prediction accuracy.

An ML-optimized 5G antenna operating in commonly used smartphone bands such as n77 and n78 is presented in [67]. The antenna operates at 3.6 GHz and 4.1 GHz with a bandwidth ranging from 3.3 GHz to 4.2 GHz. A maximum gain of 7.95 dB and a radiation efficiency of 97.67% are achieved through regression-based optimization of antenna dimensions and geometry. The high efficiency demonstrates the effectiveness of ML-assisted parameter tuning in minimizing impedance mismatch and radiation loss.

For low-power IoT applications, [51] presents a dual-state frequency reconfigurable antenna optimized using Gaussian Process Regression (GPR). The ML-assisted optimization improves surface current distribution, resulting in enhanced radiation stability across operating states, as shown in Figure 11. The predicted resonant behavior closely matches simulation results, demonstrating the effectiveness of GPR in capturing antenna characteristics. Additionally, improved Received Signal Strength Indicator (RSSI) performance compared to conventional monopole antennas highlights the practical advantage of ML-assisted design. GPR is particularly suitable for such applications due to its ability to model prediction uncertainty while maintaining high accuracy with relatively small datasets.

Other ML models have also been applied for performance prediction in reconfigurable antenna systems. The design in [50] utilizes multilayer superstrate structures to enhance radiation performance, where ML-based regression techniques significantly reduce computational cost compared to full-wave simulations. Although conventional simulation tools provide higher absolute accuracy, ML-assisted approaches enable faster optimization, making them highly effective for iterative design processes.

In [65], an ANN-based approach is employed to model frequency and return loss characteristics in a varactor-based reconfigurable antenna. ANN models are particularly effective in capturing nonlinear relationships between tuning parameters and antenna response, although their performance depends on dataset size and training quality.

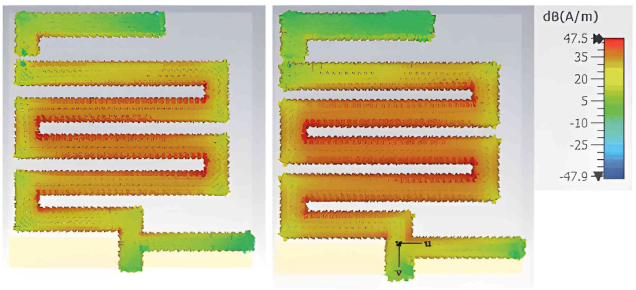

Figure 11. Surface current distribution of ML-optimized LoRa antenna reported in [51]. (a) Active mode at 868 MHz, (b) Passive mode at 915 MHz.

Random Forest Regression (RFR) is utilized in [68] to predict gain in a 28 GHz four-element MIMO array. Although the design is not frequency reconfigurable, it demonstrates ML effectiveness in high-frequency array optimization. The antenna achieves a bandwidth of 5.1 GHz, maximum gain of 9.43 dBi, isolation of 31.37 dB, and overall efficiency of 99.6%. RFR achieves gain prediction accuracy of approximately 99%, highlighting its robustness in regression tasks involving high-dimensional parameter spaces.

Comprehensive procedural explanations for ML and Deep Learning (DL) integration are provided in [69] and [70]. In [69], ANN is applied to optimize the bandwidth of a rectangular microstrip antenna. The model predicts optimal length and width parameters based on desired frequency and bandwidth inputs, demonstrating rapid geometry synthesis. In contrast, [70] employs a Deep Neural Network (DNN) to determine capacitor values required for impedance matching. By training on multiple S_{11} impedance profiles, the DNN predicts circuit parameters capable of achieving target resonance conditions, even for unconventional waveform inputs. This demonstrates the suitability of DL models for precise impedance control and inverse design problems.

Overall, ML-assisted optimization enhances antenna design by reducing computational complexity, accelerating convergence, and enabling intelligent parameter exploration. GPR is effective for uncertainty-aware frequency prediction in smaller datasets. ANNs excel in nonlinear mapping between geometry and electromagnetic response. RFR provides robust and accurate gain prediction in high-dimensional parameter spaces. Despite these advantages, ML models require carefully curated training datasets and may exhibit reduced generalization outside the trained parameter range. Therefore, ML techniques are most effective when integrated with electromagnetic simulations rather than fully replacing them.

Although lumped component-based reconfigurable antennas offer fast switching speed, compact size, and low fabrication cost, they may suffer from problems related to reduced radiation efficiency and complex biasing networks. ML-assisted optimization helps mitigate these limitations by modifying the geometric and electrical parameters to improve the impedance matching and radiation performance.

3. Mechanical reconfigurable antennas

As illustrated in Figure 2, mechanical reconfiguration enables frequency and polarization agility by physically altering antenna geometry, substrate properties, or structural alignment. Unlike lumped-element techniques, mechanical approaches generally provide high linearity, high power handling capability, and low insertion loss. However, they are inherently slower and may involve increased structural complexity.

3.1 *Structural reconfiguration (sliding, rotation, actuation)*

Sliding and displacement-based tuning methods modify the effective electrical length of the antenna through controlled mechanical motion. Mechanical sliding using rack-and-pinion actuation is demonstrated in [71], where frequency

reconfiguration is achieved by physically exposing or covering sections of the radiator, enabling dual-band operation with stable polarization characteristics.

A more advanced displacement-based approach is presented in [72], where a movable substrate slides over a fixed radiator using motor-driven actuation, as shown in Figure 12. The integration of a $\lambda/4$ reflector improves impedance matching and radiation performance, although a trade-off between bandwidth expansion and gain is observed, Figure 13.

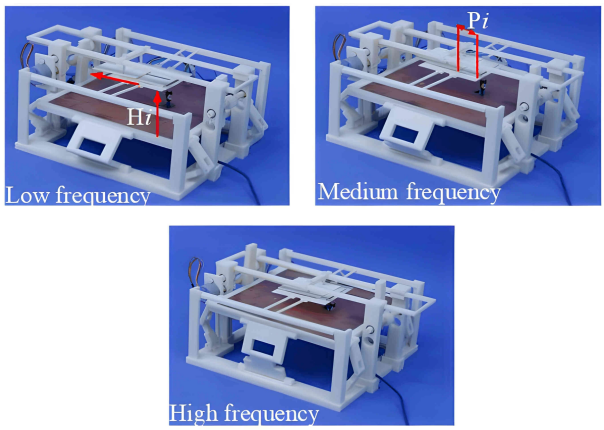

Figure 12. Mechanically reconfigurable antenna prototype for low (1.15 GHz), medium (1.73 GHz), and high (3 GHz) bands in [72] (CC BY 4.0)

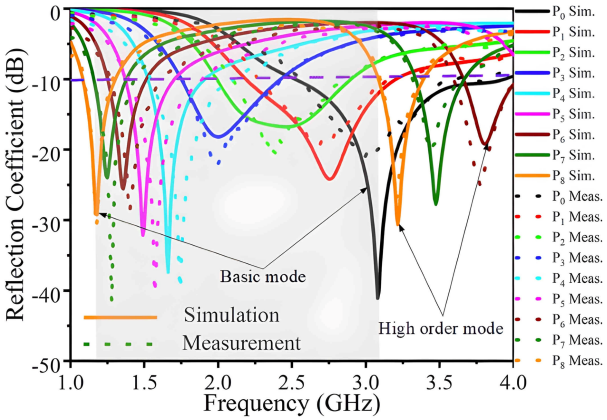

Figure 13. Simulated and measured S_{11} versus frequency for the sliding array structure in [72] (CC BY 4.0)

Similarly, mechanically controlled structures such as [73] employ variable-length radiators to achieve frequency tuning, demonstrating high power handling capability but introducing challenges such as increased back lobe radiation.

Hybrid strategies further enhance structural reconfiguration by combining mechanical motion with electromagnetic surface engineering. In [74], a rotatable metasurface enables polarization switching and gain enhancement through controlled angular displacement, where the air gap between the radiator and metasurface excites higher-order modes for improved radiation shaping.

Stretchable designs such as [75] extend mechanical reconfiguration into flexible domains, where structural deformation alters electrical connectivity and enables wide tuning ranges. These approaches highlight the versatility of structural reconfiguration techniques, although they often involve increased mechanical complexity and slower response times.

3.2 *Dielectric fluid based approaches*

Dielectric and fluidic reconfiguration techniques achieve frequency tuning by modifying the effective permittivity of the antenna environment. In [76], multiple cavities beneath the radiator are selectively filled with different dielectric materials, enabling discrete frequency tuning through controlled permittivity variation. This approach maintains stable radiation characteristics but introduces structural complexity.

A related fluidic approach is presented in [77], where liquid media are used to dynamically alter the dielectric properties beneath the antenna. While such methods provide stable radiation behavior and flexible tuning, their reliance on manual or semi-automated fluid control limits practical deployment in real-time systems.

Fluidic reconfiguration exploits dielectric variation or liquid metal displacement to achieve frequency and polarization tuning. In [78], a square patch integrates gravity-controlled liquid metal within a Polydimethylsiloxane (PDMS) structure, enabling dynamic reconfiguration without the need for conventional biasing circuits. The displacement of liquid metal modifies the effective capacitance and phase distribution, facilitating switching between different polarization states.

Such approaches offer large tuning ranges and multifunctional operation; however, they introduce practical challenges such as structural maintenance, fluid stability, and implementation complexity, which may limit their suitability for real-time or long-term deployment.

3.3 *Origami and kirigami structures*

Origami and kirigami-inspired antennas provide mechanically flexible reconfiguration suitable for wearable and deployable systems. In [79], a thermally responsive origami antenna employs a twisted S-shaped dipole on a flexible substrate, as illustrated in Figure 14. Frequency tuning is achieved through controlled folding, where changes in the effective dipole length and induced short-circuit conditions modify the resonant behavior. The structure also demonstrates self-deployment capability, highlighting its potential for adaptive systems.

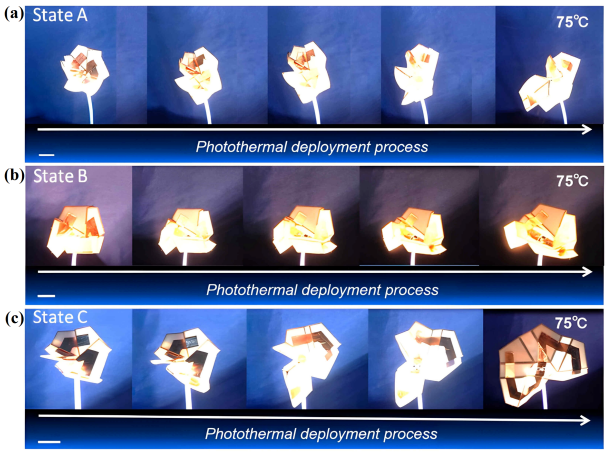

Figure 14. Self-deployment process of hexagon-twist frequency reconfigurable antenna in [79] with (a) state A, (b) state B and (c) state C under photothermal condition. (CC BY 4.0)

Kirigami-based structures further extend mechanical reconfiguration by enabling controlled structural deformation. In [80], a multi-layer kirigami configuration achieves frequency tuning through variation in the effective monopole length, demonstrating stable operation with moderate efficiency.

Advanced material-based implementations such as [81] utilize MXene-based conductive inks on flexible substrates to achieve strain-induced reconfiguration. Mechanical deformation alters the electrical properties of the structures, enabling both frequency tuning and beam steering capabilities. These approaches highlight the potential of kirigami-inspired designs in achieving multifunctional reconfiguration through material and structural synergy.

3.4 *Comparative analysis of mechanical strategies*

The mechanical techniques discussed above and summarized in Table 5 exhibit diverse tuning mechanisms governed by trade-offs between tuning depth, structural complexity, and actuation latency. As summarized in Table 6, sliding and rotational systems provide robust power handling ($>$ 40 dBm) with efficiencies between 85% and 95%, but exhibit slower switching times ranging from hundreds of milliseconds to seconds. Fluidic approaches offer the largest tuning ratios, though with moderate efficiency and maintenance requirements.The Origami and Kirigami architectures achieve moderate tuning ranges while offering superior flexibility for wearable and deployable systems. Hybrid metasurface-integrated methods enhance polarization and radiation shaping while maintaining high efficiency.

Although mechanical reconfiguration typically operates on millisecond-to-second timescales, it remains advantageous in high-linearity and high-power environments where semiconductor switches may experience thermal stress or parasitic distortion. The primary limitation remains long-term reliability of moving components and the integration of motor control mechanisms within compact antenna housings.

Table 5. Highlights of sophisticated mechanically reconfigurable antennas of Section 3

Ref	Frequency Range (GHz)	Substrate (ε_r) (height)	Overall Dimension (mm^2)	Feed Type	Radiator Shape	Reconfigurability cause	Peak Gain (dBi)	Applications
Structural movement-based reconfigurable antennas of sub-Section 3.1								
[73]	0.75–1, 1.2–1.5	Polythene (ε_r = 2.25) & Plexiglass	200 x 200 (Max height is 21.5 cm)	Network	Quadrifiliar Helix & 4 armed Yagi-Uda	3 times change in helix height	6.15, 7.3 (dB)	Cubesat
[71]	(1st design) 2 & 4, 2.2 & 4.5, 2.5 & 5, 2.8 & 5, 3 & 5.8 (2nd design) 2 & 4, 2.3 & 4.5, 2.4 & 5, 2.9	ABS (ε_r = 2.4) (h = 2.54 mm)	100 x 60	CPW	Dipole-like	Stepper motor with dual & single rack-pinion structure of designs respectively	4.5 & 6.8	Harmonic radars, in severe environments
[72]	1.15–3.08	Rogers 4350 (ε_r = 3.66) (h = 1.52 mm)	60 x 80	Coaxial	Rectangular strip, forming array	Rack & pinion with stepper motor	7.51 & 11.81	IOT, in severe environments
[74]	7.05–9.62, 5.49–9.4, 5.83–6.01	F4B (ε_r = 2.2) (h = 8 mm)	60 x 60	Tapering microstrip	Circular arc	Rotating the metasurface	9.1	sub-6G, satellite, medical communication, C & X band
[75]	2.3–7.7	FPCB (ε_r = 2.55) (h = 12 μm)	N/A	Direct	Chain of 2 orthogonal C arcs with reducing heights (Buckling process)	Tensile strength on substrate, triggering switch	N/A	Wireless/flexible electronics, UWB applications
Dielectric fluid-based reconfigurable antennas of sub-Section 3.2								
[76]	2.398–2.955 & 2.234–2.944	FR4 (ε_r = 4.4) (h = 2.4 mm)	61 x 59	Microstrip	Rectangular patch	4 cavities in substrate filled with air and rogers material	4.32 (dB)	RFID, LTE_2500, WLAN, WSN, IOT
[78]	1.2–1.6, 2.5–2.75, 4.2–4.55, 5–5.4	TQX440 (ε_r = 4.4) (h = 1.5 mm)	70 x 70	Coaxial	Square patch with strips	Gravity affected Liquid metal in Square ring PDMS structure	5.07	FDD, TDD, TD-LTE, 5G-n77, Satellite communication
[77]	2.442–2.716	FR4 (ε_r = 4.4) (h = 3.2 mm)	31 x 39	Microstrip	Rectangular patch	3 end-to-end fluidic cavities in substrate	4.39	WLAN, IOT, Wireless sensors network

Table 5. Cont.

Ref	Frequency Range (GHz)	Substrate (ε_r) (height)	Overall Dimension (mm^2)	Feed Type	Radiator Shape	Reconfigurability cause	Peak Gain (dBi)	Applications
Origami/Kirigami-based reconfigurable antennas of sub-Section 3.3								
[80]	0.42–0.53	FR4 (ε_r = 4.4) PET (er = 2.9) (h = 1.34 mm)	120 x 120 (h = 128 mm)	Direct	Vertical 3 storey kirigami monopole	Adding a storey, increasing patch length	0.76	Deployable structures
[79]	2.39–4.13	Multi-material (ε_r = 2.8) (h = 0.5 mm)	30-100 (inner-outer hexago height)	Coaxial	Twisted-S dipole	Origami-hexagon twist, temperature control	N/A	S & C band
[81]	3.5, 6.5, 9.3	Acetate film (ε_r = 1.5) (h = N/A)	100 x 65 & 145 x 105	CPW	Piano like rectangular strip	Buckling strain of kirigami & frequency selective patterns on MXene coating	N/A	ISM, S, C, X band

Note: N/A indicates Not Available.

Table 6. Quantitative performance benchmarks of mechanical reconfiguration methods

Specific Mechanism Type	Tuning Ratio (f_{max} : f_{min})	P_{1dB} (dBm)	Time (τ)	Eff. (η)	References
Rotational / Sliding	1.3:1 - 3.0:1	> 40	100 ms - 2 s	85%-95%	[71–73, 76, 77]
Fluidic / Liquid Metal	2.0:1 - 5.0:1	25 - 35	500 ms - 5 s	60%-80%	[78]
Origami / Kirigami	1.2:1 - 2.5:1	> 30	200 ms - 3 s	75%-90%	[79–81]
Structural / Metasurface	1.1:1 - 1.5:1	20 - 30	1 ms - 100 ms	80%-95%	[74, 75]

4. Metamaterial based reconfigurable antennas

Metamaterial-based reconfiguration exploits artificially engineered electromagnetic media whose effective permittivity, permeability, or surface impedance can be dynamically altered to achieve frequency agility. Unlike conventional lumped-element approaches that modify current paths through switches, metamaterial strategies manipulate the intrinsic electromagnetic response of sub wavelength unit cells. This enables frequency tuning without directly interrupting the radiating structure, resulting in improved integration, compactness, and enhanced control over antenna characteristics.

4.1 *Fundamental concepts and material platforms*

In addition to conventional metamaterial loading techniques, recent studies have explored advanced engineered transmission-line and resonator-based structures to further enhance antenna performance. Composite Right/Left-Handed (CRLH) transmission line-based antennas have demonstrated significant potential in achieving compact size, enhanced gain, and multi-resonant behaviors. These structures exploit the simultaneous presence of right-handed and left-handed propagation modes, enabling flexible control over dispersion characteristics and resonance tuning. As a result, CRLH-based designs are particularly effective for realization of miniaturized frequency reconfigurable antennas with improved bandwidth and radiation efficiency [82, 83]. Additionally, fractal-based left-handed metamaterial structures have been investigated to improve radiation characteristics and suppress undesired cross-polarization components. By incorporating self-similar geometries, these structures increase effective electrical length while maintaining compact size, leading to multiband operation and improved radiation pattern control. Their ability to enhance gain and polarization purity makes them attractive for integration into reconfigurable antenna systems [84].

4.2 *Reconfiguration mechanisms in metamaterial systems*

Metamaterial-based reconfiguration can be broadly categorized on the mechanism used to alter effective electromagnetic properties.

4.2.1 *Liquid based reconfigurability*

Fluidic and dielectric modulation techniques achieve frequency tuning by modifying the surrounding dielectric environment through controlled liquid displacement or injection [85–89]. Liquid metal-based approaches extend this concept by dynamically altering current distribution through conductive fluid movement [89], as illustrated in Figure 15 & 16. While these methods provide wide tuning ranges, they are often limited by slow response times, dielectric losses, and practical challenges such as leakage and mechanical integration.

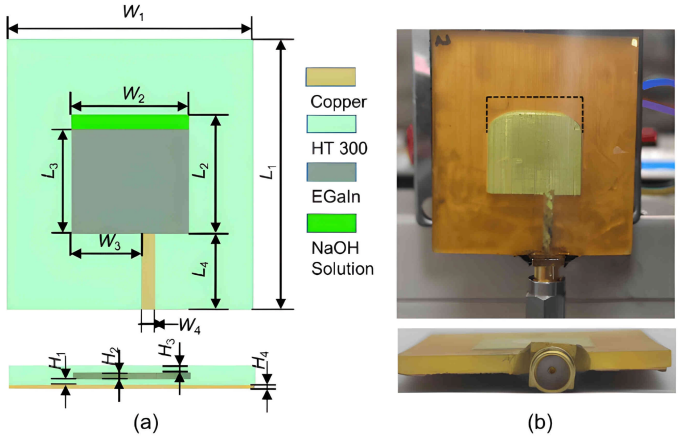

Figure 15. Gravity-controlled liquid metal reconfiguration mechanism in [89]. (a) Schematic & (b) Fabricated prototype. (CC BY 4.0)

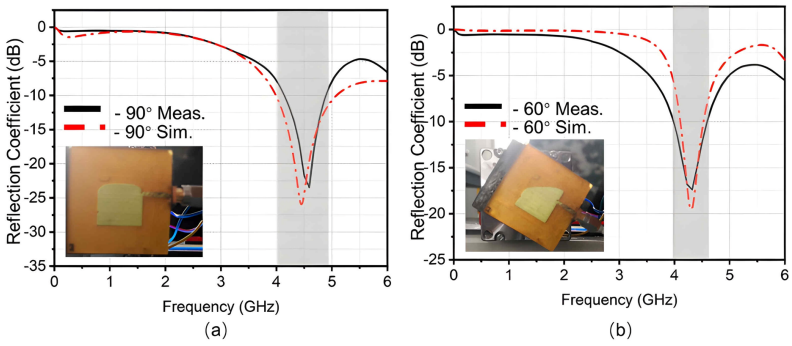

Figure 16. Effect of rotation on impedance bandwidth and return loss in [89]. (CC BY 4.0)

4.2.2 *Liquid crystal based frequency reconfiguration*

Field-driven material tuning offers an alternative approach by modifying intrinsic dielectric properties without mechanical motion. Liquid crystal-based systems of Figure 17 & 18 enables continuous frequency tuning through voltage-controlled molecular realignment, providing low-power operation and smooth frequency agility suitable for wearable and transparent electronics [90, 91].

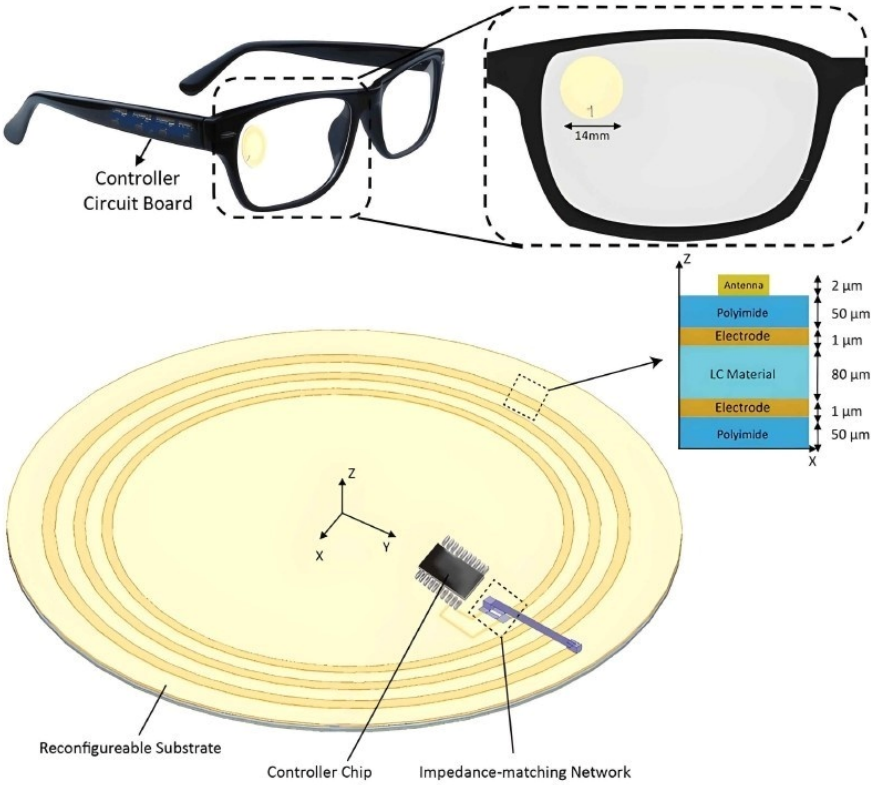

Figure 17. Multi-layer Liquid crystal based reconfigurable antenna for wearable 5G smart glasses applications. Adapted from [91] under CC BY 4.0)

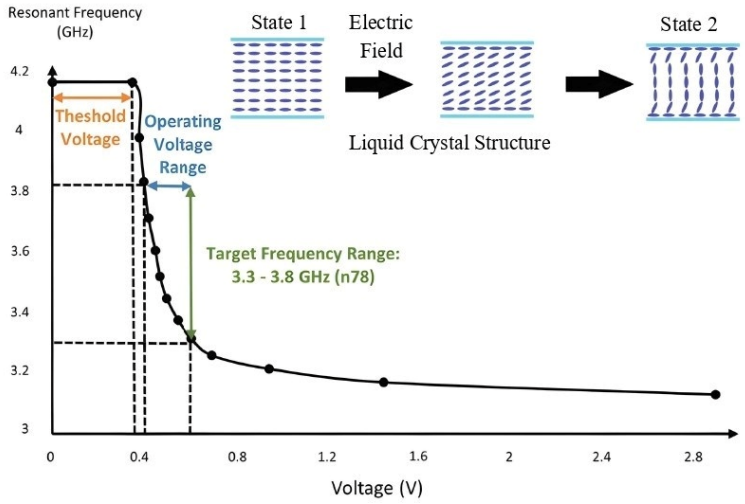

Figure 18. Resonant frequency variation versus bias voltage showing continuous tuning across the 5G n78 band with lattice structure. Adapted from [91] under CC BY 4.0

4.2.3 *Phase change materials*

Phase-change materials such as vanadium dioxide (VO_2) enable discrete switching through thermally induced conductivity transitions, supporting fast reconfiguration at higher frequencies, particularly in mmWave applications [92].

These approaches offer improved integration and faster response compared to fluidic methods, although thermal stability and fabrication precision remain important considerations.

4.2.4 *Metasurface-enabled and advanced reconfigurable architectures*

Metasurfaces represent the planar extension of metamaterials, enabling electromagnetic manipulation through engineered surface impedance and phase control. Designed as periodic arrays of subwavelength unit cells, metasurfaces provide a low-profile platform for achieving frequency reconfiguration and advanced radiation control. Recent metasurface-based antenna designs demonstrate capabilities such as polarization-insensitive reception, multi-beam transmission, and multifunctional electromagnetic behavior [93–98]. Polarization-insensitive metalenses maintain consistent phase response across orthogonal polarization states, enabling orientation-independent operation. Dual-mode transmissive metasurfaces allow simultaneous manipulation of multiple wavefronts, supporting spatial multiplexing and improved spectral efficiency. Multifunctional metasurface arrays further integrate polarization conversion, focusing, and beam shaping within a single compact structure. Mechanically induced reconfiguration techniques, including rotational unit-cell control and cavity-based tuning, modify electromagnetic coupling through structural variation. Rotational configurations alter the orientation of periodic unit cells, allowing frequency tuning through controlled changes in electromagnetic interaction [94]. Similarly, cavity-based structures such as Fabry-Perot configurations utilize interference effects between layers to achieve tunable or multi-band operation [75, 93]. While these approaches preserve radiation symmetry, they introduce additional mechanical or structural complexity. Magneto-dielectric metamaterials provide reconfiguration through externally controlled magnetic permeability. Ferrite-based structures integrated with resonant elements enable non-contact tuning via applied magnetic bias fields, resulting in stable and predictable frequency shifts [95]. However, these systems require additional biasing infrastructure, which increases overall complexity. Digitally controlled metasurfaces enable independent manipulation of polarization, phase, and wavefront characteristics through reconfigurable unit cells [94, 97], facilitating real-time adaptive antenna operation. Such multifunctional platforms integrate focus and polarization control into compact apertures [96, 98], while mechanically adaptive layers offer an alternative for high-gain tuning [93]. In parallel, transformable metamaterials inspired by kirigami introduce structural flexibility through geometric deformation engineered, enabling frequency and radiation reconfiguration without complex biasing networks [81]. These approaches reflect a shift toward hybrid reconfigurable systems that combine electromagnetic programmability with mechanical adaptability. Recent advances in metasurface engineering have introduced programmable and mechanically adaptive reconfiguration strategies that extend beyond conventional lumped-element and static metamaterial approaches. One notable development is the use of spin-decoupled programmable metasurfaces, where orthogonal polarization components can be independently controlled through digitally addressable unit cells. Such architectures enable simultaneous manipulation of reflection phase, polarization state, and wave front characteristics, thereby facilitating multifunctional antenna operation within a single compact platform. These structures are particularly relevant for next-generation adaptive communication systems, where dynamic polarization diversity and beam agility are critical [99].

In parallel, kirigami-inspired transformable metamaterials have emerged as a promising approach for mechanically driven reconfiguration. By introducing strategically engineered cuts and folds into conductive or dielectric surfaces, these structures can undergo controlled geometric transformations that directly alter their electromagnetic response. This enables real-time tuning of resonant frequency, radiation pattern, and polarization without requiring complex biasing networks. Compared to purely electrical tuning methods, kirigami-based designs offer reduced parasitic losses and enhanced structural flexibility, making them suitable for wearable, deployable, and space-constrained applications [100].

These emerging strategies highlight a shift toward hybrid reconfigurable platforms, where electrical programmability and mechanical adaptability are integrated within metasurface-based antenna systems. Such approaches provide a pathway toward low power, highly adaptive antennas capable of supporting dynamic wireless environments envisioned in 5G and future 6G systems.

4.3 *Comparative analysis of metamaterial strategies*

Tables 7 and 8 summarize the performance metrics of these approaches. Fluidic methods provide wide tuning ranges but are limited by slow response times and dielectric losses. Field-driven liquid crystals offer ultra-low voltage control with continuous tuning, making them suitable for wearable electronics. Phase-change materials such as VO_2 provide rapid switching at mmWave frequencies, though thermal management is required. Rotational metasurface configurations preserve radiation symmetry while enabling moderate tuning ratios. Magneto-dielectric substrates achieve contactless tuning but require magnetic bias systems. Left handed fractals and antenna arrays using metasurfaces are promising avenues for enhancement in antenna performance in the frequency ranges discussed in this paper. The metasurface-driven array architectures discussed above highlight the transition from conventional antenna arrays toward programmable electromagnetic apertures. Unlike traditional reconfigurable antennas that rely on discrete switching elements or mechanical actuation, metasurface arrays achieve reconfiguration through engineered phase manipulation at the unit-cell level. Polarization-insensitive metalenses provide orientation-agnostic reception by maintaining phase consistency across arbitrary polarization states, which is particularly beneficial for reflectarray systems where transmitter alignment may vary. Dual-mode transmissive metasurfaces extend this concept further by enabling simultaneous multibeam operation, allowing spatial multiplexing and improved spectral utilization in dense wireless environments. Meanwhile, multifunctional microstrip metasurface arrays demonstrate how multiple electromagnetic functions such as polarization conversion, focusing, and beam shaping can be integrated into a single compact structure. Collectively, these approaches illustrate that metasurface-based arrays offer superior aperture efficiency, reduced profile thickness, and enhanced electromagnetic control compared to traditional phased arrays, making them promising candidates for next-generation 5G, satellite communication, and emerging 6G beamforming systems.

Overall, metamaterial reconfiguration shifts the focus from discrete switching to electromagnetic property engineering. The progression from mechanical liquid displacement to solid-state phase-change and anisotropic dielectric tuning reflects a broader trend toward compact, low-power, and integration-friendly reconfigurable antenna platforms for future 5G, mmWave, and 6G systems.

Table 7. Synopsis of frontline metamaterial reconfigurable antennas of Section 4

Ref	Operating Frequencies (GHz)	Substrate (ε_r) (height)	Overall Dimensions (mm x mm)	Feed Type	Radiator Shape	Peak Gain (dBi)	Reconfiguration Technique	Applications
Liquid based Reconfiguration								
[88]	3.26 - 3.75, 5.07 - 5.9	Arlon (ε_r = 2.5) (h = 0.762 mm)	26.6 x 11.4	Microstrip	Semi-Rectangular & quarter square with circular slots	3.85-5.03	Changing number of distilled water filled vias	sub-6 GHz
[87]	2.2 - 3.75	Rogers 4003 (ε_r = 3.55) (h = N/A)	100 x 100	Microstrip	Fluidic cavity with water above patch	5.5-7.2	Water flow through fluidic cavity which provides dielectric tuning	S band, WiFi
[86]	11, 13	Quartz (ε_r = 3.9) (h = 1 mm)	Outer Radius 4.1 mm & Inner Radius 3.9 mm	CPW	Annular Ring slot	N/A	EWOD technique	Cognitive wireless communication
[89]	3.69 - 4.95	HT 300 (ε_r = 2.7) (h = 0.5 mm)	40 x 40	Microstrip	Based upon gravity	1.43	Dependent on gravity controlled movement of liquid EGaIn	5G mobile networks

Table 7. Cont.

Ref	Operating Frequencies (GHz)	Substrate (ε_r) (height)	Overall Dimensions (mm x mm)	Feed Type	Radiator Shape	Peak Gain (dBi)	Reconfiguration Technique	Applications
Liquid Crystal based Reconfiguration								
[90]	28.8 - 31.8	Taconic TLY5 (ε_r = 2.2) (h = 0.381 mm) Rogers 5880 + LC BYIPS 01 (ε_r = 2.2 + 2.74 - 5.4) (h = 0.254 mm) Aluminium (ε_r = 1) (h = 7 mm)	25 x 25	Microstrip	Slotted Rectangular Patch	6.25 & 5.54 (dB)	Deflection of liquid crystal molecules is achieved through application of external DC voltage	5G mm Wave
[91]	3.09 - 4.15	RDP 84909 (ε_r = 47.1 & 8) (h = 0.08 mm) Polyimide (h = 0.05 + 0.05 mm)	6.8 (mm^2)	Network	Spiral	N/A	Dependent on operating voltage	5G wearable applications
Phase Change Materials								
[92]	29.7, 26	Rogers 5880 (ε_r = 2.20) (h = 0.5 mm)	18 x 10	Microstrip	Square with VO_2 filled slot	6.9	Change in conductivity of VO_2 with temperature	Can be used for mmwave applications
Metasurface based Reconfiguration								
[95]	3.7, 4, 4.4	Rogers (ε_r = 2.20) (h = 3.2 mm) Ferrite NG 1850 (h = 3.2 mm)	22.5 x 6	Coaxial	H shaped	7.1 (dB)	Static magnetic magnetic field applied to ferrite substrate	Satellite communication
[94]	23 - 29.1, 23.3, 25, 27, 28.3	Rogers 5880 (ε_r = 2.2) (h = 2 mm)	2.8 x 1.8 (array of 16)	Coaxial	Rectangular patch with U shaped slot	19.7 - 19.9	Changing distance between two layers of unit cells	Radar, 5G communication
[93]	2.55 - 3.45	Rogers 5880 (ε_r = 3.38) (h = 1.524 mm)	100 x 100	CPW	Dipole	8.3 (dB)	Physical rotational movement of metasurface	Wireless application

Note: N/A indicates Not Available.

Table 8. Critical performance comparison of metamaterial and advanced material tuning strategies

Ref.	Mechanism	Tuning Agent	Frequency / States	Hardware Rationale / Drawback
[86]	EWOD (Liquid Contact Angle)	Liquid Mercury on Quartz	11 GHz (140 V) to 13 GHz (0 V)	Eliminates pumps; requires prohibitive 140 V biasing.
[91]	Molecular Realignment	RDP-84909 Liquid Crystal (LC)	3.3–3.8 GHz (0.4–0.6 V)	Ultra-low 0.36 V threshold; ideal for wearable lenses.
[87]	Near-field Environment	3D Printed Water Container	2.2–3.75 GHz (Fluid levels)	Wide range; high dielectric loss at high frequencies.
[89]	Gravity/Rotation Displacement	EGaIn Liquid Metal in NaOH	3.69–4.95 GHz (±30° to ±90°)	Simple mechanism; low gain (1.43 dBi) and complex setup.
[92]	Thermal Phase Change	VO_2 Bridge/Heater	27.6–31.8 GHz (27°C) to 24.9–27.1 GHz (75°C)	Faster mmWave switching; susceptible to overheating.
[95]	Magnetic Interaction	Ferrite Slabs with SRRs	3.7 GHz (0 mT) to 4.4 GHz (50 mT)	Precise magnetic control; high fabrication complexity.

5. Observations, advantages, challenges, and frontiers

Various antenna reconfiguration methodologies, including electrical, mechanical, metamaterial-based, and machine learning-assisted approaches, have been systematically analyzed in this review. Each technique exhibits a distinct performance envelope defined by switching speed, power handling, fabrication complexity, integration capability, and long-term reliability. The following subsections synthesize the critical observations and emerging research frontiers.

5.1 *Electrically reconfigurable antennas*

Electrical reconfiguration remains the most widely adopted methodology for frequency tuning due to its superior switching agility compared to mechanical and material-based techniques.

The radar-based comparison in Figure 19 highlights distinct performance trade-offs among electrical reconfiguration techniques. PIN diode-based designs exhibit the highest switching speed and reliability, making them well-suited for real-time and multi-band communication systems. However, their moderate insertion loss and limited linearity indicate performance constraints in high-frequency and precision applications.

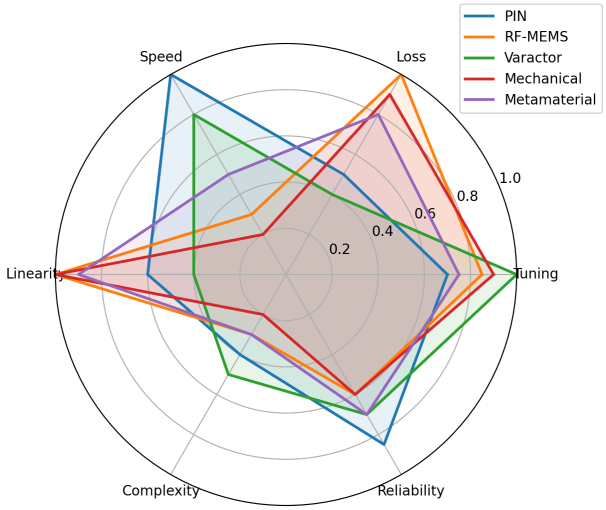

Figure 19. Radar-based comparison of FRA reconfiguration techniques using normalized performance metrics (0 (low) - 1 (high) scale)

RF-MEMS techniques demonstrate superior performance in insertion loss and linearity, achieving near-ideal characteristics for high-frequency operation. This makes them highly suitable for mmWave and radar systems, although their significantly lower switching speed limits their applicability in dynamic reconfiguration scenarios.

Varactor-based approaches show the highest tuning capability among all electrical techniques, enabling continuous frequency control and enhanced spectral agility. Their relatively high switching speed further supports adaptive communication systems. However, reduced linearity and moderate loss highlight inherent limitations due to nonlinear capacitance behavior.

Overall, the radar analysis reveals that electrical techniques offer complementary strengths: PIN diodes excel in speed and reliability, RF-MEMS in low-loss and linearity, and varactors in tuning flexibility. This reinforces that the selection of an appropriate electrical reconfiguration method is inherently dependent on the target application and required performance trade-offs.

5.1.1 *Practical implementation challenges*

Despite the advantages of electrically reconfigurable FRAs, their deployment in real-world applications remains low. This section provides an in depth insight on the causes for this scenario. Different components suffer from different kinds of challenges which pertains to their applications in diverse fields.

• **PIN diodes:** They introduce high ohmic losses in the system, which are generally proportional to the frequency of operation. The temperature of the diodes also fluctuates with the influx of heavy current, which limits their deployment in applications where stability is important. The use of PIN diodes also requires a continuous DC power supply which increases the overall power consumption of the system. The requirement of complex biasing networks increases the fabrication costs, while the introduction of parasitic capacitance and inductance reduces the efficiency of the system.

• **RF-MEMS:** They enjoy the advantage of having low insertion loss and high isolation, but these components have a limited life cycle which limits their deployment in long term applications. This type of devices have extremely low power requirements for their normal operating modes, but the voltage required for actuation is comparatively large.

• **Varactors:** They are one of the few components to provide continuous frequency tuning but they are sensitive to fluctuations in reverse bias voltage and exhibit non-linear behavior. The power consumption for this type of devices is low, but their non-linear behavior limits their applications.

5.1.2 *Frontiers*

The future research domains in this category are briefed below with further technological improvements:

• Large antenna arrays, with several elements that manage parameters such as phase, amplitude, and isolation in MIMO systems, are prone to internal parasitic effects and sometimes unpredictable behavior that hamper efficiency and performance. The behavior of individual elements in such systems needs extensive research, especially in calibration techniques.

• AI/ML can be useful in this endeavor due to the large number of parameters involved.

• The use of cognitive radio techniques can be helpful in ensuring that the antenna operates optimally in any environment. Analysis of the effect of well-known metal compounds on antenna performance by replacing traditional lumped elements.

5.2 *Mechanically reconfigurable antennas*

Mechanical frequency reconfiguration remains a high-performance alternative to semiconductor-based switching, primarily attributing to its ability to provide diverse operational modes without the insertion losses associated with lumped components. Although conventional mechanical systems are often associated with bulkier structures and millisecond-to-second switching latency, advances in material science are steadily pushing this technology toward compact, low-profile implementations.

Mechanical reconfiguration techniques demonstrate strong performance in tuning capability, insertion loss, and linearity, as evident from the radar comparison of Figure 19. These approaches achieve near-ideal values in linearity and low-loss operation, highlighting their suitability for high-efficiency and high-gain antenna systems. Their wide tuning range further enables flexible operation across multiple frequency bands.

A critical observation derived from the eleven mechanical strategies reviewed in Section 3 is the emerging role of material-driven reconfiguration. Specifically, the integration of high-conductivity nanomaterials, such as $Ti_3C_2T_x$ MXene ($> 10^4$ S/cm), on flexible acetate substrates enables structural tuning that rivals the efficiency of metallic radiators. The use of Kirigami-inspired buckling mechanisms allows for significant frequency shifts (up to 400 MHz) and dynamic beam steering (up to 24°) while maintaining a thin-film profile that addresses the historical "bulkiness" bottleneck.

5.2.1 *Practical deployment challenges*

These antennas offer better efficiency and wider tuning ranges than their electrical counterparts; the physical movement of various parts is the main source of limitations for this type. The primary deployment challenges are as follows:

• **Mechanical Fatigue:** Since reconfiguration is based on bending, rotation, displacement, or folding, the components are constantly under stress. In Origami or Kirigami structures, repetitive folding can lead to microscopic cracks in the substrate or the conductive traces which can lead to electrical failure.

• **Reliability:** Actuators such as motors, piezoelectric actuators among many others have a finite number of cycles before they wear out which is a major concern for long time applications

• **Slow Switching Speed:** Compared to electrical frequency reconfiguration methods(PIN diodes, Varactors etc), mechanical methods are inherently slow. This makes mechanical reconfiguration techniques unsuitable for mm wave applications

5.2.2 *Frontiers*

• **Satellite and Space Platforms:** Mechanically reconfigurable antennas enable high-gain and frequency-agile operation in CubeSats and deployable systems, where structural adaptability and efficiency are critical.

• **Adaptive and Harsh Environment Systems:** Rack-and-pinion and displacement-based designs provide reliable tuning in extreme conditions where electronic components may suffer from thermal or radiation effects.

• **Fluidic and Soft Reconfigurable Systems:** Liquid-metal and dielectric-fluid-based antennas support multifunctional reconfiguration, including frequency and polarization tuning, for flexible and emerging soft electronic platforms.

• **Metasurface-Assisted Beam and Polarization Control:** Mechanically actuated metasurfaces enable dynamic beam shaping and polarization switching, supporting advanced communication and sensing applications.

5.3 *Metamaterial based reconfigurable antennas*

Metamaterial-driven reconfiguration, encompassing LCs, phase-change materials (PCM), functional fluids, and magneto-dielectric substrates, represents a promising pathway toward compact, low-profile tuning architectures. As summarized in Table 8, material selection is governed by frequency band requirements, voltage constraints, response time, and integration feasibility, the selection rationale for these materials is primarily governed by the required frequency band and the available power budget. For instance, while liquid-based approaches like EWOD enable rapid switching by altering contact angles via external DC voltage, the requirement for high potentials ($>$140 V) limits their portability in consumer electronics. In contrast, the integration of RDP-84909 Liquid Crystals enables ultra-low-voltage (0.4–0.6 V) frequency tuning throughout the 5G n78 band, making it a superior candidate for wearable applications such as intelligent glass lenses.

A critical observation from the current research landscape is the transition from liquid displacement to solid-state phase-change mechanisms for mmWave and 6G applications. The use of vanadium dioxide (VO_2) ink bridges provides high isolation and rapid switching speeds ($<$ ms) compared to microfluidic systems, which are inherently limited by the time required for physical fluid transport. Furthermore, the introduction of magnetic control via ferrite-embedded SRRs offers a path toward precise, contactless frequency modulation.

Recent developments in metasurface-based antenna arrays further expand the scope of metamaterial-driven reconfiguration. Unlike tunable material approaches that rely on dielectric or phase-change properties, metasurface arrays enable dynamic electromagnetic control through engineered phase distributions across sub-wavelength unit cells. Architectures such as polarization-insensitive metalenses, dual-mode transmissive metasurfaces, and multifunctional microstrip arrays demonstrate how metasurfaces can simultaneously achieve beam focusing, polarization conversion, and multi-beam transmission within compact structures. These capabilities position metasurface arrays as a promising platform for highly efficient beamforming and spatial multiplexing in future 5G and 6G communication systems.

5.3.1 *Practical deployment challenges*

While metamaterial-based antennas (including Metasurfaces, CRLH, and Fractal structures) overcome many size and efficiency barriers of traditional antennas, they introduce a unique set of technical and fabrication limitations [101].

• **Phase Change Materials:** They require precise temperature control, which limits their usability in volatile environments.

• **Liquid Metals:** Introduce mechanical instability and risk of leakage. They also require additional setup for the use of motors for rotation or any other equipment, which makes the setup bulky, limiting application in areas where size is a major concern.

• **Substrate Materials:** They may suffer from frequency de-tuning due to variation in permittivity, bending, humidity, or temperature, especially in wearable antennas. This limits the application of this type of antennas in wearable applications. Also, multi-layered substrates require sophisticated manufacturing processes, which leads to increase in fabrication cost, and reduction in scalability for mass production.

5.3.2 *Frontiers*

The analysis concludes that future advancements should prioritize the following research frontiers:

• **High-Frequency Dielectric Optimization:** Development of specialized dielectric liquids and metamaterial substrates with lower loss tangents to overcome the efficiency limitations of water-based designs at mm wave frequencies.

• **Fluidic Response Latency:** Engineering sophisticated micro-capillary mechanisms or utilizing gravity-controlled liquid metal (EGaIn) displacement to reduce system response time or eliminate complex pumping hardware altogether.

• **Thermal and Reliability Management:** Integration of enhanced thermal control mechanisms and precision-printed VO_2 layers to mitigate the risk of heat damage during high-temperature (e.g., 75°C) ON-state operations.

The comparison of top-performing antennas across different reconfiguration techniques is provided in Table 9 which highlights distinct performance trade-offs. PIN diode-based designs demonstrate strong versatility and wideband capability, while RF-MEMS approaches enable ultra-wide tuning ranges suitable for mmWave applications. Varactor-based antennas provide continuous frequency tuning, making them ideal for cognitive radio systems. Mechanical and fluidic techniques achieve high gain and multifunctional reconfiguration but are limited by slower response times. Metamaterial-based designs exhibit superior gain performance and precise control, particularly in high-frequency applications. These observations indicate that the choice of reconfiguration technique is highly application-dependent, with no single approach providing optimal performance across all metrics. Figure 20 mentions the KPIs of each reconfiguration technique discussed in this paper and its suitable applications.

Table 9. Cross-technology comparison of top performing reconfigurable antennas

Ref	Technique	Freq. Range	Gain (dBi)	Key Feature	Insight	Application
[55]	PIN	1.33-8.7 GHz	10.13	UWB + multiband	High gain with wide coverage; strong candidate for multi-standard systems	UWB, 5G sub-6 GHz, WLAN
[42]	PIN (MIMO)	2.5-14 GHz	6.2	Wideband MIMO	Excellent spectral flexibility; suitable for modern communication systems	5G, MIMO systems, cognitive radio
[33]	PIN	27-32 GHz	9.1	Beam steering	Combines mmWave operation with radiation control	5G mmWave, beamforming systems
[58]	RF-MEMS	7.6-31 GHz	–	Large array	Extremely wide tuning; scalable for mmWave arrays	mmWave arrays, satellite, radar
[60]	Varactor	5-6.6 GHz	5.2	Continuous tuning	Smooth frequency agility; suitable for cognitive radio	Cognitive radio, sub-6 GHz 5G
[39]	PIN	2.4-19 GHz	8	Multiband (17 states)	High reconfigurability; trade-off with complexity	ISM, WLAN, LTE, multi-band systems
[72]	Mechanical	1.15-3 GHz	11.8	Sliding + array	Highest gain; strong for adaptive platforms	IoT, adaptive communication, harsh environments
[74]	Mechanical (Meta)	5.4-9.6 GHz	9.1	Rotating metasurface	High efficiency with polarization control	Satellite, sub-6 GHz, polarization-agile systems

Table 9. Cont.

Ref	Technique	Freq. Range	Gain (dBi)	Key Feature	Insight	Application
[78]	Fluidic	1.2-5.4 GHz	5.07	Polarization switching	Multifunctional tuning without biasing	5G, satellite, multi-mode communication
[94]	Metamaterial	23-29 GHz	19.9	High-gain array	Exceptional gain for mmWave applications	5G mmWave, radar
[90]	Metamaterial	28.8-31.8 GHz	6.25	Liquid crystal tuning	Precise control for mmWave tuning	5G mmWave, tunable RF front-ends

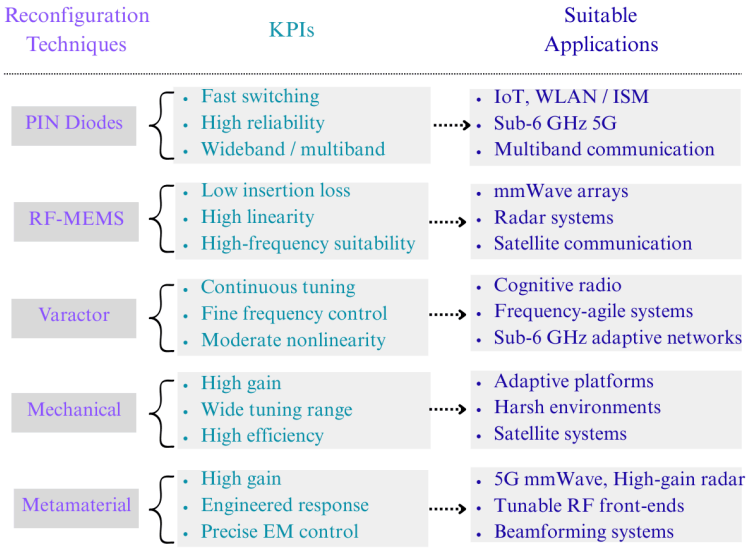

Figure 20. Mapping of FRA reconfiguration techniques to Key Performance Indicators (KPIs) and applications

5.4 *Machine Learning based assistance*

Machine Learning algorithms represent a transformative paradigm for optimizing parameters such as impedance matching, RLC values prediction, bandwidth enhancement, and frequency prediction. These models achieve high practical efficiency and can reduce resource utilization by up to 80% compared to traditional simulation software. However, the rationale behind selecting a specific algorithm is vital (Table 10): GPR is chosen for its probabilistic reliability with small datasets, while ANN is selected for its predictive power in complex, data-rich environments.

Despite the promising capabilities of ML in antenna design, several challenges limit its widespread adoption in FRA systems. One major limitation is the scarcity of high-quality datasets, as generating training data requires extensive full-wave electromagnetic (EM) simulations, which are computationally expensive. This restricts the scalability of ML models and limits their applicability to diverse antenna geometries. Another critical challenge is the generalization capability of ML models. Most existing approaches are trained on specific antenna configurations and may not perform reliably when applied to unseen geometries or different reconfiguration mechanisms. This limits the robustness of ML-assisted design in practical scenarios.

Furthermore, the integration of ML models with full-wave EM solvers remains an open challenge. While ML can accelerate parameter optimization, achieving seamless end-to-end design workflows that combine ML prediction with EM validation is still an active area of research.

The future of machine learning-assisted FRA design lies in addressing current limitations while enabling more robust, efficient, and adaptive antenna optimization frameworks to meet the rigorous demands of next-generation 5G/6G wireless networks [106].

Table 10. Summary of best use cases of ML algorithms with their strengths and weaknesses

Algorithm	Best Use Case in Antenna Design	Strength	Weakness	Rationale for Selection
Artificial Neural Network (ANN) [102]	Inverse design & geometrical optimization	Models high non-linearity	Requires massive datasets	Chosen when accuracy is priority over interpretability.
Gaussian Process Regression (GPR) [103]	Surrogate modeling with sparse data	Provides uncertainty / confidence intervals	Computationally heavy for large data ($O(n^3)$)	Chosen when the simulations are extremely time-consuming (e.g. array antennas).
Support Vector Regression (SVR) [104]	High-dimensional parameter spaces	Robust to noisy simulation data	Hard to tune hyperparameters	Chosen for robust prediction in smaller datasets.
Random Forest Regression (RFR) [105]	Gain/Bandwidth prediction & Sensitivity analysis of parameters	Identifies key design parameters	Poor extrapolation beyond training range	Chosen to understand which physical dimensions drive performance.

5.4.1 *Frontiers for existing challenges*

• Development of transfer learning techniques to address dataset scarcity and enable efficient reuse of pre-trained models for diverse FRA geometries.

• Integration of machine learning with full-wave electromagnetic (EM) solvers to establish hybrid ML-EM design workflows for accurate and efficient end-to-end optimization.

• Incorporation of physics-informed machine learning to embed electromagnetic constraints into the learning process and enhance prediction accuracy.

• Development of lightweight ML models for deployment in resource-constrained environments such as IoT and wearable systems.

• Investigation of automated data generation and augmentation techniques to reduce dependency on computationally expensive simulation datasets.

The Table 11 highlights trade-offs between accuracy, computational cost, and data requirements, emphasizing that model selection depends on application constraints.

Table 11. Compact comparison of ML and optimization techniques for FRA design

Technique	Accuracy	Computational Cost	Dataset size	Key Insights
GPR	High (RMSE ~0.05)	Moderate (O(n^3))	Low	Accurate for small datasets; provides uncertainty; poor scalability
ANN	Very High (R^2 >0.95)	High	High	Captures nonlinear EM behavior; best accuracy; risk of overfitting
RFR / SVR	Moderate-High	Low-Moderate	Moderate	Robust and fast; suitable for rapid design; limited extrapolation
DT / LASSO	Low-Moderate	Very Low	Low	Useful for feature selection; not suitable for complex FRA modeling
GA / PSO	Optimization-based	High	None	Global search capability; requires many EM simulations; slow convergence
RL	Emerging	Very High	Very High	Enables real-time adaptive tuning; still immature for FRA applications

6. Conclusion

This paper has presented a comprehensive and performance-driven analysis of frequency reconfigurable antenna techniques, encompassing electrical, mechanical, and metamaterial-based approaches, along with emerging machine learning integration. The comparative evaluation highlights that electrical techniques provide fast and practical reconfiguration, mechanical approaches enable high gain and linearity, and metamaterial-based designs offer compactness and precise electromagnetic control, each exhibiting distinct trade-offs across key performance metrics.

In the context of next-generation wireless systems, FRA development must align with the stringent requirements of 6G, including mmWave/terahertz operation, ultra-massive MIMO, and adaptive spectrum utilization. To address these challenges, future research should focus on (i) developing low-loss and highly reliable RF-MEMS for high-frequency applications, (ii) optimizing tunable metamaterials such as liquid crystal and phase-change materials for low-voltage and wearable systems, and (iii) designing ML-driven frameworks for real-time adaptive frequency tuning in dynamic wireless environments.

Furthermore, viable hybrid reconfiguration architectures, such as electrical-mechanical and metamaterial-ML integrated systems, should be explored to combine fast switching, wide tunability, and intelligent control. These directions establish a clear pathway for advancing FRA technologies toward fully adaptive, high-efficiency, and self-optimizing communication systems suitable for 6G, satellite, and cognitive radio applications.

Acknowledgment

The authors thank PVG College of Engineering, Technology and Management for institutional support and the Defense Institute of Advanced Technology (DIAT) for guidance and technical assistance. The authors also acknowledge the anonymous reviewers for their constructive comments that improved this manuscript.

Conflict of interest

The authors declare no conflict of interest.

References

[1] X. Lu, E. Sopin, V. Petrov, O. Galinina, D. Moltchanov, K. Ageey. et al., "Integrated use of licensed-and unlicensed-band mmWave radio technology in 5G and beyond," *IEEE Access*, vol. 7, pp. 24376–24391, 2019. https://doi.org/10.1109/ACCESS.2019.2900195.

[2] R. R. Kunath, R. Q. Lee, K. S. Martzaklis, K. A. Shalkhauser, A. N. Downey, and R. N. Sinons, *An optically controlled Ka-band phased array antenna*. Solid State Technology Branch of NASA Lewis Research Center Fourth Annual Digest, 1992, pp. 35.

[3] J. Boyns, C. Gorham, A. Munger, J. Provencher, J. Reindel, and B. Small, "Step-scanned circular-array antenna," *IEEE Transactions on Antennas and Propagation*, vol. 18, no. 5, pp. 590–595, 1970. https://doi.org/10.1109/TAP.1970.1139762.

[4] D. H. Schaubert, F. G. Farrar, S. T. Hayes, and A. R. Sindoris, "Frequency-agile, polarization diverse microstrip antennas and frequency scanned arrays," U.S. Patent 4,367,474, Jan. 1983.

[5] J. T. Bernhard, *Reconfigurable Antennas*. San Rafael, CA, USA: Morgan & Claypool Publishers, 2007.

[6] G. Kumar and K. P. Ray, *Broadband Microstrip Antennas*. Norwood, MA, USA: Artech House, 2003.

[7] P. Katehi and N. Alexopoulos, "On the effect of substrate thickness and permittivity on printed circuit dipole properties," *IEEE Transactions on Antennas and Propagation*, vol. 31, no. 1, pp. 34–39, 1983. https://doi.org/10.1109/TAP.1983.1143003.

[8] L. C. Paul, M. S. Hosain, S. Sarker, M. H. Prio, M. Morshed, and A. K. Sarkar, "The effect of changing substrate material and thickness on the performance of inset feed microstrip patch antenna," *American Journal of Networks and Communications*, vol. 4, no. 3, pp. 54–58, 2015. https://doi.org/10.11648/j.ajnc.20150403.16.

[9] S. F. Farida, P. M. Hadalgi, P. V. Hunagund, and S. R. Ara, "Effect of substrate thickness and permittivity on the characteristics of rectangular microstrip antenna," In Proc. Conference on Precision Electromagnetic Measurements Digest, Washington, DC, USA, Jul. 6–10, 1998, pp. 598–599. https://doi.org/10.1109/CPEM.1998.700074.

[10] J. T. Rayno and S. K. Sharma, "Effect of substrate thickness on the performance of a printed planar monopole antenna (PMA)," In Proc. IEEE International Symposium on Antennas and Propagation, Chicago, IL, USA, Jul. 8–14, 2012, pp. 1–2. https://doi.org/10.1109/APS.2012.6348659.

[11] A. Bhattacharyya and R. Garg, "Effect of substrate on the efficiency of an arbitrarily shaped microstrip patch antenna," *IEEE Transactions on Antennas and Propagation*, vol. 34, no. 10, pp. 1181–1188, 2003. https://doi.org/10.1109/TAP.1986.1143748.

[12] N. Kumar, P. Kumar, and M. Sharma, "Reconfigurable antenna and performance optimization approach," *Wireless Personal Communications*, vol. 112, no. 4, pp. 2187–2212, 2020. https://doi.org/10.1007/s11277-020-07145-0.

[13] M. K. Abdulhameed, M. S. M. Isa, I. M. Ibrahim, M. K. Mohsin, S. R. Hashim, and M. L. Attiah, "Improvement of microstrip antenna performance on thick and high permittivity substrate with electromagnetic band gap," *Journal of Advanced Research in Dynamic and Control Systems*, vol. 10, no. 4, pp. 661–669, 2018.

[14] S. Noghanian and L. Shafai, "Control of microstrip antenna radiation characteristics by ground plane size and shape," *IEE Proceedings-Microwaves, Antennas and Propagation*, vol. 145, no. 3, pp. 207–212, 1998.

[15] Z. N. Chen, T. S. P. See, and X. Qing, "Small printed ultrawideband antenna with reduced ground plane effect," *IEEE Transactions on Antennas and Propagation*, vol. 55, no. 2, pp. 383–388, 2007. https://doi.org/10.1109/TAP.2006.889823.

[16] M.-C. Huynh and W. Stutzman, "Ground plane effects on planar inverted-F antenna (PIFA) performance," *IEE Proceedings-Microwaves, Antennas and Propagation*, vol. 150, no. 4, pp. 209–213, 2003.

[17] K. P. Ray and Y. Ranga, "Ultrawideband printed elliptical monopole antennas," *IEEE Transactions on Antennas and Propagation*, vol. 55, no. 4, pp. 1189–1192, 2007. https://doi.org/10.1109/TAP.2007.893408.

[18] P. V. Anob, K. P. Ray, and G. Kumar, "Wideband orthogonal square monopole antennas with semi-circular base," In Proc. IEEE Antennas and Propagation Society International Symposium, Boston, MA, USA, Jul. 8-13, 2001, pp. 294–297. https://doi.org/10.1109/APS.2001.960090.

[19] N. P. Agrawall, G. Kumar, and K. P. Ray, "Wide-band planar monopole antennas," *IEEE Transactions on Antennas and Propagation*, vol. 46, no. 2, pp. 294–295, 1998. https://doi.org/10.1109/8.660976.

[20] J. P. Gianvittorio and Y. Rahmat-Samii, "Fractal antennas: a novel antenna miniaturization technique, and applications," *IEEE Antennas and Propagation Magazine*, vol. 44, no. 1, pp. 20–36, 2002. https://doi.org/10.1109/74.997888.

[21] A. A. Deshmukh and K. P. Ray, "Compact broadband slotted rectangular microstrip antenna," *IEEE Antennas and Wireless Propagation Letters*, vol. 8, pp. 1410–1413, 2009. https://doi.org/10.1109/LAWP.2010.2040061.

[22] D. M. Pozar, "A reciprocity method of analysis for printed slot and slot-coupled microstrip antennas," *IEEE Transactions on Antennas and Propagation*, vol. 34, no. 12, pp. 1439–1446, 1986. https://doi.org/10.1109/TAP.1986.1143785.

[23] K. Da Xu, H. Xu, Y. Liu, J. Li, and Q. H. Liu, "Microstrip patch antennas with multiple parasitic patches and shorting vias for bandwidth enhancement," *IEEE Access*, vol. 6, pp. 11624–11633, 2018. https://doi.org/10.1109/ACCESS.2018.2794962.

[24] T. M. Au and K. M. Luk, "Effect of parasitic element on the characteristics of microstrip antenna," *IEEE Transactions on Antennas and Propagation*, vol. 39, no. 8, pp. 1247–1251, 1991. https://doi.org/10.1109/8.97366.

[25] S. K. Jain and P. K. Jain, "Machine learning-driven antenna design," in *Array and Wearable Antennas: Design, Optimization, and Applications*. Boca Raton, FL, USA: CRC Press, 2024, p. 72.

[26] H. M. El Misilmani, T. Naous, and S. K. Al Khatib, "A review on the design and optimization of antennas using machine learning algorithms and techniques," *International Journal of RF and Microwave Computer-Aided Engineering*, vol. 30, no. 10, p. e22356, 2020. https://doi.org/10.1002/mmce.22356.

[27] N. Sarker, P. Podder, M. R. H. Mondal, S. S. Shafin and J. Kamruzzaman, et al., "Applications of machine learning and deep learning in antenna design, optimization and selection: a review," *IEEE Access*, vol. 11, pp. 103890–103915, 2023. https://doi.org/10.1109/ACCESS.2023.3317371.

[28] N. Hussain, A. Ghaffar, S. I. Naqvi, A. Iftikhar, D. E. Anagnostou, H. H. Tran, "A conformal frequency reconfigurable antenna with multiband and wideband characteristics," *Sensors*, vol. 22, no. 7, p. 2601, 2022. https://doi.org/10.3390/s22072601.

[29] S. M. Salleh, M. Jusoh, A. H. Ismail, M. R. Kamarudin, P. Nobles, M. K. A. Rahim, et al., "Textile antenna with simultaneous frequency and polarization reconfiguration for WBAN," *IEEE Access*, vol. 6, pp. 7350–7358, 2017. https://doi.org/10.1109/ACCESS.2017.2787018.

[30] B. R. Sanjeeva Reddy, N. K. Darimireddy, C.-W. Park, and A. Chehri, "Performance of reconfigurable antenna fabricated on flexible and nonflexible materials for band switching applications," *Energies*, vol. 14, no. 9, p. 2553, 2021. https://doi.org/10.3390/en14092553.

[31] P. Saha, D. Mitra, and S. K. Parui, "A frequency and polarization agile disc monopole wearable antenna for medical applications," *Radioengineering*, vol. 29, no. 1, pp. 123–130, 2020. https://doi.org/10.13164/re.2020.0074.

[32] I. Ahmad, H. Sun, Y. Zhang, and Q. Ali, "Low profile, compact size frequency reconfigurable antenna for 5G mm-wave wireless communication," In Proc. International Conference on Computer and Communication Systems, Shanghai, China, May 15–18, 2020, pp. 712–716. https://doi.org/10.1109/ICCCS49078.2020.9118458.

[33] F. Arshad, A. Ali, J. Loo, Y. Amin, and H. Tenhunen, "Beam-width agile antenna for 5G MMW applications," In Proc. International Conference on UK-China Emerging Technologies, Glasgow, UK, Aug. 20–21, 2020, pp. 1–5. https://doi.org/10.1109/UCET51115.2020.9205358.

[34] K. Karthika and K. Kavitha, "Design and development of parasitic elements loaded quadband frequency and pattern reconfigurable antenna," *International Journal of RF and Microwave Computer-Aided Engineering*, vol. 2023, no. 1, p. 4034241, 2023. https://doi.org/10.1155/2023/4034241.

[35] S. A. Aghdam, "Reconfigurable antenna with a diversity filtering band feature utilizing active devices for communication systems," *IEEE Transactions on Antennas and Propagation*, vol. 61, no. 10, pp. 5223–5228, 2013. https://doi.org/10.1109/TAP.2013.2273812.

[36] M. S. Yahya, S. Soeung, N. S. S. Singh, Z. Yunusa, F. E. Chinda, S. K. A. Rahim, et al., "Triple-band reconfigurable monopole antenna for long-range IoT applications," *Sensors*, vol. 23, no. 12, p. 5359, 2023. https://doi.org/10.3390/s23125359.

[37] A. A. Jabber and R. H. Thaher, "Compact tri-band T-shaped frequency reconfigurable antenna for cognitive radio applications," *Bulletin of Electrical Engineering and Informatics*, vol. 9, no. 1, pp. 212–220, 2020. https://doi.org/10.11591/eei.v9i1.1708.

[38] K. Karthika and K. Kavitha, "Design and development of self-complementary DNA structure-based frequency reconfigurable antenna," *Journal of Electrical Engineering & Technology*, vol. 19, pp. 5247–5258, 2024. https://doi.org/10.1007/s42835-024-01917-5.

[39] M. A. Shuriji and R. H. Thaher, "A reconfigurable switching diode loaded patch antenna for S, C, X, Ku, and K bands applications," *Bulletin of Electrical Engineering and Informatics*, vol. 13, no. 1, pp. 247–253, 2024. https://doi.org/10.11591/eei.v13i1.5738.

[40] H.-H. Tran, P. Kim-Thi, T. T.-L. Nguyen, and H. T. P. Thao, "A flexible and bandwidth reconfigurable antenna for cognitive communication," *IEEE Access*, vol. 11, pp. 45678–45689, 2023. https://doi.org/10.1109/ACCESS.2023.3306451.

[41] J. Qin, X. Fu, M. Sun, Q. Ren, and A. Chen, "Frequency reconfigurable antenna based on substrate integrated waveguide for S-band and C-band applications," *IEEE Access*, vol. 9, pp. 2839–2845, 2020. https://doi.org/10.1109/ACCESS.2020.3047540.

[42] A. H. Jabire, H. M. AlkhoorI, A. Ghaffar, Y. S. Faouri, A. Dahir, M. I. Hussein, "Frequency and pattern reconfigurable CPW-fed MIMO antenna with multiband and wideband characteristics," *IEEE Access*, vol. 12, pp. 12345–12358, 2024. https://doi.org/10.1109/ACCESS.2024.3450868.

[43] J. Kumar, B. Basu, F. A. Talukdar, and A. Nandi, "Graphene-based multimode inspired frequency reconfigurable user terminal antenna for satellite communication," *IET Communications*, vol. 12, no. 1, pp. 67–74, 2018. https://doi.org/10.1049/iet-com.2017.0253.

[44] S. T. Al-Hadeethi, T. A. Elwi, and A. A. Ibrahim, "A printed reconfigurable monopole antenna based on a novel metamaterial structures for 5G applications," *Micromachines*, vol. 14, no. 1, p. 131, 2023. https://doi.org/10.3390/mi14010131.

[45] H. Rajagopalan, J. M. Kovitz, and Y. Rahmat-Samii, "MEMS reconfigurable optimized E-shaped patch antenna design for cognitive radio," *IEEE Transactions on Antennas and Propagation*, vol. 62, no. 3, pp. 1056–1064, 2013. https://doi.org/10.1109/TAP.2013.2292531.

[46] D. Rodrigo, B. A. Cetiner and L. Jofre, "Frequency, radiation pattern and polarization reconfigurable antenna using a parasitic pixel layer," *IEEE Transactions on Antennas and Propagation*, vol. 62, no. 6, pp. 3422–3427, 2014. https://doi.org/10.1109/TAP.2014.2314464.

[47] M. Hussain, E. M. Ali, W. A. Awan, N. Hussain, M. Alibakhshikenari, B. S. Virdee, et al., "Electronically reconfigurable and conformal triband antenna for wireless communications systems and portable devices," *PLOS ONE*, vol. 17, no. 12, 2022. https://doi.org/10.1371/journal.pone.0276922.

[48] N. A. Jazea, A. K. Jassim, and A. K. Hassan, "Design and analysis of frequency reconfigurable antenna for global positioning system applications," *Bulletin of Electrical Engineering and Informatics*, vol. 11, no. 1, pp. 248–255, 2022. https://doi.org/10.11591/eei.v11i1.3234.

[49] A. Varshney, T. M. Neebha, V. Sharma, J. G. Jency, and A. D. Andrushia, "Dodecagon-shaped frequency reconfigurable antenna practically loaded with 3-delta structures for ISM band and wireless applications," *IETE Journal of Research*, vol. 69, no. 11, pp. 7747–7759, 2023. https://doi.org/10.1080/03772063.2022.2034536.

[50] S. K. Patel, J. Surve, V. Katkar, and J. Parmar, "Machine learning assisted metamaterial-based reconfigurable antenna for low-cost portable electronic devices," *Scientific Reports*, vol. 12, no. 1, 2022. https://doi.org/10.1038/s41598-022-16678-2.

[51] M. S. Yahya, S. Soeung, S. K. A. Rahim, U. Musa, S. S. Ba Hashwan and M. A. Haque, "Machine learning-optimized compact frequency reconfigurable antenna with RSSI enhancement for long-range applications," *IEEE Access*, vol. 12, pp. 10970–10987, 2024. https://doi.org/10.1109/ACCESS.2024.3355145.

[52] D. N. Gençoğlan, Ş. Çolak, and M. Palandöken, "Spiral-resonator-based frequency reconfigurable antenna design for sub-6 GHz applications," *Applied Sciences*, vol. 13, no. 15, p. 8719, 2023. https://doi.org/10.3390/app13158719.

[53] K. Thenkumari, K. S. Sankaran, and J. M. Mathana, "Design and implementation of frequency reconfigurable antenna for Wi-Fi applications," *Engineered Science*, vol. 23, no. 2, p. 876, 2023. https://doi.org/10.30919/es8d876.

[54] J. Deng, S. Hou, L. Zhao, and L. Guo, "Wideband-to-narrowband tunable monopole antenna with integrated bandpass filters for UWB/WLAN applications," *IEEE Antennas and Wireless Propagation Letters*, vol. 16, pp. 2734–2737, 2017. https://doi.org/10.1109/LAWP.2017.2743258.

[55] M. Jenath Sathikbasha and V. Nagarajan, "Design of multiband frequency reconfigurable antenna with defected ground structure for wireless applications," *Wireless Personal Communications*, vol. 113, pp. 867–892, 2020. https://doi.org/10.1007/s11277-020-07256-8.

[56] S. P. Lavadiya, V. Sorathiya, S. Kanzariya, B. Chavda, A. Naweed, O. S. Faragallah, et al., "Low profile multiband microstrip patch antenna with frequency reconfigurable feature using PIN diode for S, C, X, and Ku band applications," *International Journal of Communication Systems*, vol. 35, no. 9, p. e5141, 2022. https://doi.org/10.1002/dac.5141.

[57] R. K. Saraswat and M. Kumar, "A vertex-fed hexa-band frequency reconfigurable antenna for wireless applications," *International Journal of RF and Microwave Computer-Aided Engineering*, vol. 29, no. 10, p. e21893, 2019. https://doi.org/10.1002/mmce.21893.

[58] M. Donelli, J. Iannacci, and M. Manekiya, "A new concept of reconfigurable antenna structure based on an array of RF-MEMS switches," *Applied Sciences*, vol. 14, no. 23, pp. 1–14, 2024. https://doi.org/10.3390/app142310941.

[59] E. Erdil, K. Topalli, M. Unlu, O. A. Civi, and T. Akin, "Frequency tunable microstrip patch antenna using RF MEMS technology," *IEEE Transactions on Antennas and Propagation*, vol. 55, no. 4, pp. 1193–1196, 2007. https://doi.org/10.1109/TAP.2007.893426.

[60] Q. H. Kareem, L. W. Abdullah, R. A. Shihab, F. A. J. Al-Hasani, and S. N. Abdullah, "Optimize the performance of reconfigurable antenna based on laser treatment for sub-6GHz applications," *Progress in Electromagnetics Research Letters*, vol. 123, pp. 95–103, 2025. https://doi.org/10.2528/PIERL24100702.

[61] H. A. Atallah, A. B. Abdel-Rahman, K. Yoshitomi, and R. K. Pokharel, "Compact frequency reconfigurable filtennas using varactor loaded T-shaped and H-shaped resonators for cognitive radio applications," *IET Microwaves, Antennas & Propagation*, vol. 10, no. 9, pp. 991–1001, 2016. https://doi.org/10.1049/iet-map.2015.0700.

[62] C. Guo, L. Deng, J. Dong, T. Yi, C. Liao, S. Huang, et al., "Variode enabled frequency-reconfigurable microstrip patch antenna with operation band covering S and C bands," *Progress in Electromagnetics Research M*, vol. 88, pp. 159–167, 2020. https://doi.org/10.2528/PIERM19110204.

[63] S. S. Al-Bawri, M. T. Islam, K. Hossain, T. Sabapathy, M. Jusoh, "Left-handed characteristics tunable C-shaped varactor loaded textile metamaterial for microwave applications," *Computers, Materials, & Continua*, vol. 71, no. 1, pp. 611-628, 2022. https://doi.org/10.32604/cmc.2022.021244.

[64] Y. P. Selvam, L. Elumalai, M. G. N. Alsath, M. Kanagasabai, S. Subbaraj, and S. Kingsly, "Novel frequency-and pattern-reconfigurable rhombic patch antenna with switchable polarization," *IEEE Antennas and Wireless Propagation Letters*, vol. 16, pp. 1639–1642, 2017. https://doi.org/10.1109/LAWP.2017.2660069.

[65] M. Yusuf, N. D. Bhandare, S. A. N. A and S. Roy, "A machine learning based design of frequency reconfigurable compact microstrip patch antenna," In Proc. IEEE Microwaves, Antennas, and Propagation Conference, Ahmedabad, India, Dec. 11–14, 2023, pp. 1–4. https://doi.org/10.1109/MAPCON58678.2023.10463931.

[66] T. Li, H. Zhai, L. Li, and C. Liang, "Frequency-reconfigurable bow-tie antenna with a wide tuning range," *IEEE Antennas and Wireless Propagation Letters*, vol. 13, pp. 1549–1552, 2014. https://doi.org/10.1109/LAWP.2014.2344676.

[67] M. A. Haque, M. A. Rahman, S. S. Al-Bawri, K. Aljaloud, N. S. S. Singh, D. Saha, et al., "Machine learning-based approach for bandwidth and frequency prediction for N77 band 5G antenna," *Physica Scripta*, vol. 99, no. 2, p. 026005, 2024. https://doi.org/10.1088/1402-4896/ad1d40.

[68] M. A. Haque, J. H. Nirob, K. H. Nahin, N. M. Jizat, M. A. Zakariya, R. A. Ananta, et al., "Machine learning-based technique for gain prediction of mm-wave miniaturized 5G MIMO slotted antenna array with high isolation characteristics," *Scientific Reports*, vol. 15, no. 1, p. 276, 2025. https://doi.org/10.1038/s41598-024-84182-w.

[69] S. K. Jain, "Bandwidth enhancement of patch antennas using neural network dependent modified optimizer," *International Journal of Microwave and Wireless Technologies*, vol. 8, no. 7, pp. 1111–1119, 2016. https://doi.org/10.1017/S1759078715000616.

[70] J. H. Kim and J. Bang, "Antenna impedance matching using deep learning," *Sensors*, vol. 21, no. 20, p. 6766, 2021. https://doi.org/10.3390/s21206766.

[71] I. T. Nassar, H. Tsang, D. Bardroff, C. P. Lusk, and T. M. Weller, "Mechanically reconfigurable, dual-band slot dipole antennas," *IEEE Transactions on Antennas and Propagation*, vol. 63, no. 7, pp. 3267–3271, 2015. https://doi.org/10.1109/TAP.2015.2423699.

[72] A. M. Sadiq, M. Liu, X. Zhang, Y. Luo, Y. Chen and K. Ma, "Single-motor controlled mechanically frequency reconfigurable unidirectional antenna array with stable radiation patterns," *IEEE Open Journal of Antennas and Propagation*, vol. 5, no. 6, pp. 1773–1785, 2024. https://doi.org/10.1109/OJAP.2024.3456252.

[73] Y. Tawk, "Physically controlled CubeSat antennas with an adaptive frequency operation," *IEEE Antennas and Wireless Propagation Letters*, vol. 18, no. 9, pp. 1892–1896, 2019. https://doi.org/10.1109/LAWP.2019.2932474.

[74] X. Song, A. Dong, X. Li, Y. Zhang, H. Lin, Y. Li, et al., "Gain-enhanced and mechanical reconfigurable slot antenna with metasurface," *The Applied Computational Electromagnetics Society Journal*, vol. 38, no. 8, pp. 602–608, 2023. https://doi.org/10.13052/2023.ACES.J.380807.

[75] F. Liu, X. Cheng, F. Zhang, Y. Chen, H. Song, Y. Huant, et al., "Design and assembly of reconfigurable 3D radio-frequency antennas based on mechanically triggered switches," *Advanced Electronic Materials*, vol. 5, no. 6, p. 1900256, 2019. https://doi.org/10.1002/aelm.201900256.

[76] P. Mathur, G. Madanan, and S. Raman, "Mechanically frequency reconfigurable antenna for WSN, WLAN, and LTE 2500 based internet of things applications," *International Journal of RF and Microwave Computer-Aided Engineering*, vol. 31, no. 2, p. e22318, 2021. https://doi.org/10.1002/mmce.22318.

[77] A. Raveendran, P. Mathur, and S. Raman, "Mechanically frequency reconfigurable antenna and its application as a fluid level detector for wireless sensor networks," In Proc. URSI Asia-Pacific Radio Science Conference, New Delhi, India, Mar. 9–15, 2019, pp. 1–4. https://doi.org/10.23919/URSIAP-RASC.2019.8738663.

[78] L. Li, X. Yan, H. C. Zhang, and Q. Wang, "Polarization-and frequency-reconfigurable patch antenna using gravity-controlled liquid metal," *IEEE Transactions on Circuits and Systems II: Express Briefs*, vol. 69, no. 3, pp. 1029–1033, 2021. https://doi.org/10.1109/TCSII.2021.3119040.

[79] Y.-J. Zhang, L.-C. Wang, W.-L. Song, M. Chen, and D. Fang, "Hexagon-twist frequency reconfigurable antennas via multi-material printed thermo-responsive origami structures," *Frontiers in Materials*, vol. 7, p. 600863, 2020. https://doi.org/10.3389/fmats.2020.600863.

[80] S. Lee, M. Lee, and S. Lim, "Frequency reconfigurable antenna actuated by three-storey tower kirigami," *Extreme Mechanics Letters*, vol. 39, p. 100833, 2020. https://doi.org/10.1016/j.eml.2020.100833.

[81] O. Niksan, L. Bi, Y. Gogotsi, and M. H. Zarifi, "MXene-based kirigami designs: showcasing reconfigurable frequency selectivity in microwave regime," *Nature Communications*, vol. 15, no. 1, p. 7793, 2024. https://doi.org/10.1038/s41467-024-51853-1.

[82] C. Caloz and T. Itoh, *Electromagnetic Metamaterials: Transmission Line Theory and Microwave Applications*. Hoboken, NJ, USA: John Wiley & Sons, 2005. https://doi.org/10.1002/0471754323.

[83] G. V. Eleftheriades, "A generalized negative-refractive-index transmission-line (NRI-TL) metamaterial for dual-band and quad-band applications," *IEEE Microwave and Wireless Components Letters*, vol. 17, no. 6, pp. 415–417, 2007. https://doi.org/10.1109/LMWC.2007.897786.

[84] J. Banerjee, A. Karmakar, R. Ghatak, and D. R. Poddar, "Compact CPW-fed UWB MIMO antenna with a novel modified Minkowski fractal defected ground structure (DGS) for high isolation and triple band-notch characteristic," *Journal of Electromagnetic Waves and Applications*, vol. 31, no. 15, pp. 1550–1565, 2017. https://doi.org/10.1080/09205071.2017.1354727.

[85] A. S. M. Sayem, A. Lalbakhsh, K. P. Esselle, G. Moloudian, J. L. Buckley and R. B. V. B. Simorangkir, et al., "Advancements, challenges, and prospects of water-filled antennas," *IEEE Access*, vol. 11, pp. 8301–8323, 2023. https://doi.org/10.1109/ACCESS.2023.3238571.

[86] Y. Damgaci and B. A. Cetiner, "A frequency reconfigurable antenna based on digital microfluidics," *Lab on a Chip*, vol. 13, no. 15, pp. 2883–2887, 2013. https://doi.org/10.1039/C3LC50275A.

[87] Z. Chen, H.-Z. Li, H. Wong, W. He, J. Ren, T. Yuan, "A frequency-reconfigurable dielectric resonator antenna with a water layer," *IEEE Antennas and Wireless Propagation Letters*, vol. 22, no. 6, pp. 1456–1460, 2023. https://doi.org/10.1109/LAWP.2023.3246110.

[88] R. K. Barik, X. Wu, X. Liu, and S. Koziel, "An extremely compact frequency reconfigurable self-diplexing antenna employing dielectric liquids," *IEEE Antennas and Wireless Propagation Letters*, vol. 23, no. 11, pp. 3749–3753, 2024. https://doi.org/10.1109/LAWP.2024.3429499.

[89] P. Qin, G.-L. Huang, J.-J. Liang, Q.-Y. Wang, J.-H. Fu, X.-Y. Zhu, et al., "A gravity-triggered liquid metal patch antenna with reconfigurable frequency," *Micromachines*, vol. 12, no. 6, p. 701, 2021. https://doi.org/10.3390/mi12060701.

[90] P. Chen, D. Wang, L. Wang, L. Liu, and Z. Gan, "Liquid crystal-based reconfigurable antenna for 5G millimeter-wave," *Scientific Reports*, vol. 14, no. 1, p. 16646, 2024. https://doi.org/10.1038/s41598-024-67714-2.

[91] Y. Xia, M. Yuan, A. Dobrea, C. Li, H. Heidari, N. Mottram, et al., "Reconfigurable wearable antenna for 5G applications using nematic liquid crystals," *Nano Select*, vol. 4, no. 8, pp. 513–524, 2023. https://doi.org/10.1002/nano.202200209.

[92] S. Ma, W. Yang, J. Li, Q. Xue, and W. Che, "Millimeter-wave reconfigurable antenna based on VO_2 ink achieved by a simple process," *Materials & Design*, vol. 245, p. 113583, 2025. https://doi.org/10.1016/j.matdes.2025.113583.

[93] B. Majumder, K. Krishnamoorthy, J. Mukherjee, and K. P. Ray, "Frequency-reconfigurable slot antenna enabled by thin anisotropic double layer metasurfaces," *IEEE Transactions on Antennas and Propagation*, vol. 64, no. 4, pp. 1218–1225, 2016. https://doi.org/10.1109/TAP.2016.2526081.

[94] X. Liu, X. Wang, G.-M. Yang, D. Xiang, and L.-R. Zheng, "Dual-band frequency reconfigurable metasurface antenna for millimeter wave joint communication and radar sensing systems," *Optics Express*, vol. 32, no. 8, pp. 13851–13863, 2024. https://doi.org/10.1364/OE.522684.

[95] M. Al-Omari, H. Attia, K. K. Qureshi, and S. I. M. Sheikh, "Design of frequency-reconfigurable antenna on dielectric and magnetic metamaterial composite substrate," *IEEE Antennas and Wireless Propagation Letters*, vol. 22, no. 4, pp. 943–947, 2022. https://doi.org/10.1109/LAWP.2022.3230827.

[96] H.-X. Xu, S. Wang, C. Wang, M. Wang, Y. Wang and Q. Peng, "Polarization-insensitive metalens and its applications to reflectarrays with polarization diversity," *IEEE Transactions on Antennas and Propagation*, vol. 70, no. 3, pp. 1895–1905, 2021. https://doi.org/10.1109/TAP.2021.3112553.

[97] H.-X. Xu, T. Cai, Y.-Q. Zhuang, Q. Peng, G.-M. Wang and J.-G. Liang, "Dual-mode transmissive metasurface and its applications in multibeam transmitarray," *IEEE Transactions on Antennas and Propagation*, vol. 65, no. 4, pp. 1797–1806, 2017. https://doi.org/10.1109/TAP.2017.2673814.

[98] H.-X. Xu, S. Tang, G.-M. Wang, T. Cai, W. Huang, Q. He, et al., "Multifunctional microstrip array combining a linear polarizer and focusing metasurface," *IEEE Transactions on Antennas and Propagation*, vol. 64, no. 8, pp. 3676–3682, 2016. https://doi.org/10.1109/TAP.2016.2565742.

[99] C. Wang, F. Zhang, H.-X. Xu, T. Liu, and Z. Wang, "Dynamical multipolarized reflectarray antenna using spin-decoupled programmable metasurface," *IEEE Antennas and Wireless Propagation Letters*, vol. 23, no. 7, pp. 2036–2040, 2024. https://doi.org/10.1109/LAWP.2024.3378227.

[100] H.-X. Xu, M. Wang, G. Hu, S. Wang, Y. Wang, C. Wang, et al., "Adaptable invisibility management using kirigami-inspired transformable metamaterials," *Research*, vol. 2021, p. 9806789, 2021. https://doi.org/10.34133/2021/9806789.

[101] K. Zhang, P. J. Soh, and S. Yan, "Meta-wearable antennas-a review of metamaterial based antennas in wireless body area networks," *Materials*, vol. 14, no. 1, p. 149, 2021. https://doi.org/10.3390/ma14010149.

[102] C. Maeurer, P. Futter, and G. Gampala, "Antenna design exploration and optimization using machine learning," In Proc. European Conference on Antennas and Propagation, Copenhagen, Denmark, Mar. 15–20, 2020, pp. 1–5. https://doi.org/10.23919/EuCAP48036.2020.9135530.

[103] J. P. Jacobs, "Efficient resonant frequency modeling for dual-band microstrip antennas by Gaussian process regression," *IEEE Antennas and Wireless Propagation Letters*, vol. 14, pp. 337–341, 2014. https://doi.org/10.1109/LAWP.2014.2362937.

[104] X. W. Dai, M. Da Li, H. T. Wu, and Y. H. Zhang, "Design of compact patch antenna based on support vector regression," *Radioengineering*, vol. 31, no. 3, pp. 345–352, 2022. https://doi.org/10.13164/re.2022.0339.

[105] N. Kurniawati, D. N. N. Putri, and Y. K. Ningsih, "Random forest regression for predicting metamaterial antenna parameters," In Proc. International Conference on Industrial Electrical and Electronics, Lombok, Indonesia, Oct. 20–21, 2020, pp. 174–178. https://doi.org/10.1109/ICIEE49813.2020.9276899.

[106] IEEE Antennas and Propagation Society, "Special issue on machine learning in antenna design, modeling, and measurements," 2025. [Online]. Available: https://tinyurl.com/yrxav5zz. [Accessed Mar. 3, 2025].